The genesis of Hurricane Nate and its interaction with a nearby environment of very dry air

Blake Rutherford [1], Timothy Dunkerton [1], Michael Montgomery [2], and Scott Braun [3]

[1]Northwest Research Associates, Redmond, WA
[2]Naval Postgraduate School, Monterey, California
[3]NASA

Correspondence to: Blake Rutherford (blake@nwra.com)

Overview of changes made in the revised manuscript

We have carefully considered all of the comments from the reviewers and we have made a revised manuscript. There were some primary concerns of the reviewers that have driven the following major changes to the manuscript,

1. The concern about isobaric versus isentropic coordinates has been addressed by including a motivation for the choice of an isobaric coordinate system, and by including manifolds for the WRF simulation in isentropic coordinates. The similarity of manifolds in these two coordinate systems is consistent with our previous results.

2. The issue of sensitivity of manifolds has been addressed in many places including in the Conclusions.

3. The role of Tropical Storm Lee in establishing the synoptic environment has been expanded with an additional Figure 2(a) showing Lee and the attracting line that divides the contents of the pre-Nate region into R_1 originating from the Lee flow and R_2 with southern Gulf of Mexico origins.

4. Elliptical Lagrangian boundaries are now included in the revised manuscript. Definitions are given of a Lagrangian vortex core and shear sheath, and images of these features are overlaid on Figure 2.

5. Some of the weaker sections including the backward trajectory analysis have been greatly improved.

The changes to the text are included in our responses to each of the reviewers, and are included below. The major changes stated above as well as the many small changes suggested by the reviewers have been included in the revised manuscript, and the edited text is marked in blue.

Authors responses to review by Dave Ahijevych for "The genesis of Hurricane Nate and its interaction with a nearby environment of very dry air"

General Comments This paper extends the marsupial paradigm of tropical cyclogenesis to a non-African Easterly Wave. Without a wave-centric reference frame, air parcels around the storm are divided into two camps: those inside the pouch and *outside. It is shown that some mixing occurs across the pouch boundary due to lobes breaking off, but dry air is shielded from the inner vortex by a shearing sheath that can be traced back to the manifolds that separate pouch and non-pouch air. I almost cut my review short because I had never heard of the word 'manifold' outside of a car engine setting, but after reading through the paper, which is fairly well written, I now have a decent idea of what it means. Now that I've read the paper, the abstract and introduction make much more sense. Later in the paper there is a weaker section with some mistakes in the figure and text, but overall this is ready for publication. My technical corrections are the main component of this review. Some of the paper is still way beyond my area of expertise, and I have no idea whether it is right or wrong, such as the section on 'Manifold computations' (pages 7-8).*

We appreciate the reviewer's comments and have revised the manuscript so that all of these comments are addressed. The revised version improves the results section and provides a more thorough introduction so that a reader without expertise in Lagrangian manifolds can follow more easily. The reviewer's specific comments are given below in italic while the author's responses follow in regular font.

Specific comments

After rereading the abstract it isn't clear why source the 'tilting' mechanism is given such prominence. It is barely mentioned again in the paper.

We have removed mention of the tilting mechanism from the abstract.

The adjective 'layer-wise' used in the abstract and other places is confusing. Could you replace 'layer-wise advection' with 'advection on a constant pressure level'?

We have replaced 'layer-wise' with 'advection on a constant pressure level' and removed the term 'layer-wise' from the manuscript

Page 3, line 5. It isn't clear what 'non-advective fluxes' are. This becomes apparent later on, but it is first mentioned here without any explanation.

We have explained what non-advective fluxes are at this point in the manuscript.

Page 9, line 15. It is not obvious that the pouch region that originated from Lee still contains high potential vorticity air. From the figure, PV is muddled and similar to the PV in the portion with Gulf origins.

A new figure has been added that shows the PV from Lee from an earlier time, and the attracting line that differentiates the regions R_1 and R_2. The air contained in R_1 clearly shows the source high PV air from Lee that enters the pre-Nate region.

Technical corrections

Page 3, footnote 2. Change 'if' to 'of'.

We have made the correction.

Page 7, Figure 1 caption. Change 'L2' to 'L4'.

We have corrected the labels in the figure and text.

Page 7, line 9. What is an 'LCS'?

LCS is an acronym for Lagrangian Coherent Structure, which we have added to the paper.

Page 7, line 10. What is 'FTLE'?

FTLE is an acronym for Finite-time Lyapunov exponent, which we have added to the paper.

Page 8, line 29. U2 is never labeled in the figure. That would be nice.

U2 is now labeled in the figure.

Page 9, line 2, 3rd-to-last word. Change 'northeast' to 'southwest'.

We have made the correction.

Page 9, line 6, last term should be S1(I4,H1), not S2(I4,H1).

We have made the correction.

Page 9, footnote 7. What is 'VS'?

VS is an acronym for vorticity substance, which we have added to the paper.

Page 10, line 19. Can the lobe labels of L3 and L4 in Figure 2 (a) be reversed so as to match the order of the labels in Fig. 1? In other words, change L3 to L4 and change L4 to L3?

We have reversed the lobe labels on Figure 1 to match those in the remainder of the paper.

Page 10, line 25. Explicitly reference Fig. 2 after mentioning the gradient of theta-e. I was incorrectly looking for it (theta-e) in Fig. 3.

A reference to Figure 2 has been added where θ_e is mentioned.

Page 10, line 26. 'north' should not be capitalized.

We have made the correction.

Page 12, Figure 3 caption. Is the satellite panel described accurately? The text says it is 0.6 um, but isn't that visible? Wouldn't that be white for clouds? Not sure what the units are of the color table and it isn't clear how it could be 0.6 um imagery.

The GOES imagery shown is 3.9 μm shortwave radiation, and cold clouds are indicated by lower values. We have converted the data to temperature (K) in the revised paper. The units and description have been corrected in the text and the caption.

Page 13, Line 21. Manifolds are overlaid on water vapor not vorticity in Figure 5.

We have made this correction to indicate that the manifolds are overlaid on water vapor.

Page 14, first paragraph. Fig doesn't seem to go with text. Text talks about 700 mb vorticity and area. Figure has circulation and mean vorticity. Figure would also benefit from un-squished text. Y-axis ranges of panel (a) should be same as panel (b).

The Figure reference in the text has been changed to Figure 10. Panels (a) and (b) have been combined onto a single plot so that a comparison between the two simulations can be more easily made.

Page 14, line 18. Panel labels don't start with (a) in text reference or actual Figure 8.

We have corrected the figure labels.

Page 14, last paragraph. This paragraph is confusing. In line 21, when you say 'as the vorticity moves inward', do you mean the vorticity maximum (in the radial profile) is moving inward? And in line 27 what is meant by 'the stability of the unstable manifold'?

We have changed the text to indicate that vorticity increases toward center due to the convergent flow. We were referring to the stability of the flow along the unstable manifold, which switches from stretching to shearing during entrainment. This point has been clarified in the revised manuscript.

Fig 10, and Page 15, line 28. I think this time range is Sep 6 to 8, but can't read the time labels on some panels.

We have corrected the time range in the text and in the figure caption, and have moved the time labels or changed colors in many of the figures so that they are more readable.

Page 16, line 6. The term 'limit cycle' is first used. I was not familiar with it, but I understand it now after reading further.

The term limit cycle is now clearly defined at this point in the paper.

Page 16, lines 8-10. Something with wrong with references to Fig. 9 (c)-(h), which don't exist.

The reference should be to Figure 10 (c)-(h) and this error has been corrected.

Page 20, Fig. 8. Need units in figure or caption.

We have added units in the caption.

Author's responses to review by Anonymous Referee #2 for "The genesis of Hurricane Nate and its interaction with a nearby environment of very dry air"

This is the author's responses to the review by Anonymous Referee #2 for "The genesis of Hurricane Nate and its interaction with a nearby environment of very dry air". The authors would like to thank the referee for comments, and we feel that we have been able to address all of the areas of concern in the revised version of this paper. These comments have been used to improve the quality of this paper, and our responses to each of the individual comments is given below. The referee comments are given in italic while the author's responses are given in standard font.

Validity of 2D analysis: The manuscript provides little motivation why analysis of Lagrangian boundaries of the quasi-horizontal flow should provide insight into the development of Nate (2011). Certainly, the authors make some assumptions that they had articulated in earlier work. These assumptions, however, should be stated also in this manuscript. Importantly, the 2D assumption seems to be in contrast with a statement made by the authors about the role of convection in lobe transport (pg 13, line 28). Clarification is required. Nate develops near the boundary between two air masses. The authors emphasize the large moisture gradient across this boundary. Arguably, the very dry air to the North of Nate is of midlatitude origin and presumably this air mass is also considerably colder than the tropical air mass in which Nate develops. In short, I expect a strong baroclinic zone to the North of Nate and the large-scale, 2D flow follows isentropic rather than isobaric surfaces. I question that the analysis on isobaric surfaces is indeed Lagrangian, in the sense that the authors follow air parcels transported by the large-scale (adiabatic) flow, which is most likely one of the nonarticulated assumptions made by the authors. Convincing justification for the use of an isobaric framework in the presence of strong baroclinicity is needed.

We agree with the reviewer that both baroclinic contributions and vertical motions from convection bring into question the validity of the assumption of 2D velocities. Convection acts to increase the vertical vorticity while decreasing the area and leaving the circulation within any Lagrangian loop, including lobes, unchanged. Thus, the use of 2D velocities in a flow with convection still captures the advective changes to the circulation. The use of isobaric coordinates rather than isentropic coordinates does not change the validity of horizontal velocities used to advect material curves, but only contributes a non-advective flux of vorticity proportional to the pressure vertical velocity (Haynes and McIntyre, 1987). Along the unstable manifold segment that is aligned with the frontal boundary, the tilting flux is approximately 20% of the magnitude of total vorticity flux which includes the advective flux and the increase in circulation due to contraction of the vortex. The precise computation of these fluxes will be discussed in greater detail in a future paper. In the revised manuscript, we have included isentropic manifolds at the 315 K level, and notice that despite some vertical motions along the frontal boundary, there is no topological change in the manifolds, and only small changes in the fine structure.

The authors focus on the objective identification of hyperbolic Lagrangian structures. Similar methods can be applied to identify elliptical Lagrangian structures, which play an important role in separating a vortex from its environment also. The authors appreciate this role by their qualitative discussion of the 'shear sheet', e.g. on page 6. For a wave's critical layer (e.g. Dunkerton et al. 2009) there is conceptual understanding why the flow boundaries that arise from the environmental flow, and are thus the relevant boundaries, in which the embryo tropical cyclone develops, are hyperbolic structures. Such conceptual background misses for non-AEWs disturbances like pre-Nate, or at least the authors do not provide such background. Therefore, an objective identification of elliptical boundaries will considerably strengthen this manuscript. In addition, the identification of elliptic boundaries would help to introduce the concept of a limit cycle, which is referred to later in the manuscript, and help to define the core of the disturbance, which is undefined in the current version of the manuscript.

We thank the referee for suggesting a further discussion of elliptic Lagrangian boundaries. Much of our discussion in this paper is on the hyperbolic boundaries that are present when there is no distinguished reference frame or hyperbolic structures in that reference frame resulting from the wave flow. The elliptic boundaries are present in all cases of cyclogenesis whether a parent wave is present or not, and in the case of AEW flows, the elliptic structures are located close to closed streamlines in the wave-relative frame interior to the hyperbolic structures. In mature cyclones, elliptic boundaries do play a role in protecting the vortex from its environment because hyperbolic structures do not persist until the point of axisymmetrization. However, elliptic structures protect a developing vortex core from air that has passed through the outer pouch boundary. We have added a description of objective elliptic boundaries, their mathematical definitions, and the concept of a limit cycle to Section 2. These elliptic boundaries are now shown along with the manifolds in Figure 2. The location of the regions of high shear and of solid-body rotation at the core support our previous discussion, and help to show how the shear sheath interior to the outer pouch and external to the core protects the core from air that has penetrated the outer pouch.

pg 1, line 15; vorticity generation by tilting: This aspect is hardly touched on in this manuscript. I recommend omitting reference to this process in the abstract (and in the conclusions).

We have removed reference to the tilting mechanism in the abstract, and 'tilting' does not appear in the conclusions.

pg 5, line 1; and elsewhere; 'Eulerian boundary': There are references in the manuscript to Eulerian streamline patterns that are not illustrated in this manuscript. In addition, there are references to the role of tropical cyclone Lee that are not illustrated either. For the reader, it is rather hard to follow (and appreciate) these descriptions. I suggest using one or two additional figures to illustrate such points; or to keep such references to a minimum.

We have added an additional figure (2a) showing TS Lee and the regions of high PV from Lee that contribute to Nate. The Eulerian streamlines are not important in any part of our analysis, and there is no distinguished reference frame in which to view the Eulerian streamlines. so we have not included them. The Lagrangian boundaries from Lee make it clear that the Lagrangian boundaries, and not the Eulerian boundaries, are those relevant for the transport of vorticity from the Lee flow to the Nate development region.

pg 7, The subsection 'Manifold computations' requires considerable improvements: The authors use phrases like 'some situations' and 'additional options' but it remains unclear if or when other options are used or what methods are applied in other situations. Most importantly, it remains unclear from this description for how long the underlying trajectories have been calculated. It is well known that finite-time Lagrangian coherent structures are sensitive to the integration time. A more explicit discussion of this integration time and a discussion of the sensitivity of the results to integration time are needed.

This section has been improved by removing vague statements and by explicitly stating the length of integration time used in both in obtaining the initial curve segments and in advecting the curves. We now also discuss the sensitivity of Lagrangian boundaries to integration time and explain that a 2-3 day integration is required to achieve a closed pouch, while longer integrations increase the amount of filamentation.

pg 10, 'Relation of Lagrangian ...': Unfortunately, the presentation of the results deteriorates rather significantly from here on. E.g., the authors note that PV and O3 is shown and then continue with a discussion of θ_e, the GOES imagery is presented without units, convergence is presumably confused with confluence (pg. 13, line 1), results from WRF at 600 mb (which should read hPa) are compared to results from ECMWF data at 700 hPa, vorticity is confused with mixing ratio in Fig. 5, it is unclear what the difference is between individual panels in Figs. 4-6, : : : The subsection 'Backward trajectories' is very dense and it seems as some important information is not given to the reader. I cannot identify in the figures several features described by the authors. This is of particular importance with respect to the vertical similarity of manifolds and the limit cycle.

The results from page 10 on have been improved significantly. In particular, the above concerns have all been addressed in the revised manuscript. PV and O3 are now discussed where they are first mentioned, and the discussion of θ_e now follows after that discussion. We have converted the GOES data to temperature (K), and corrected the description and units in both the text and the figure caption. We have changed 'convergent' to 'confluent' to describe the flow along the unstable manifold.

We have now computed the manifolds for the WRF simulation at the $\eta = 0.7$ level to make a proper comparison with the ECMWF 700 hPa analysis, and the analysis at $\eta = 0.7$ has also been included for the SST sensitivity and non-divergent experiments.

The text reference to Figure 5 has been corrected to state that the mixing ratio is shown. The different panels in Figures 4 and 6 now show time-evolving manifolds overlaid on vertical vorticity. The labels on the figures and reference in the text have been improved in the new manuscript. The time labels are now easier to read so that the individual panels are easier to distinguish.

The backward trajectory section has been expanded to make it easier to follow, and each of the panels is now discussed individually and in greater detail. We have also provided further details on how the trajectories were integrated. Key features have been labeled on the trajectory plots.

The comparison between the ECMWF and the WRF data is confusing. Importantly, it is not clear how much the results based on the ECMWF data can be trusted. Furthermore, the comparison of the results using the full wind field and the non-divergent flow only is poorly motivated.

The non-divergent wind field is used to demonstrate that convergent flow is not necessary for a pouch boundary to be closed, and is unnecessary for the formation of lobes. However, the size of the lobes that intrude is far greater for convergent flow. We have made the comparison between the ECMWF data and the WRF data more clear, and now state that the ECMWF data show large non-advective fluxes, but has approximately the same topology as the WRF data. While the resolution of the ECMWF data may lead to errors in the fine-scale filaments, the manifolds still closely follow the gradients of tracers such as O_3, indicating that this data is sufficient to capture the larger-scale transport including the lobe transport prior to extreme filamentation.

The conclusions refer to several aspects that have not been discussed sufficiently in the manuscript. The arguments given in enumerations 1) and 2) are plausible but have not been shown in this manuscript. The 'core' referred to in enumeration 5) has never been defined. Finally, the Eulerian streamlines noted on pg 19 have not been shown in this manuscript. The revised conclusions should focus much more on results and insight that is shown and developed in the manuscript at hand.

With the improvements in the revised manuscript, all of the ideas discussed in the Conclusions have now been discussed in the main manuscript in sufficient detail. Arguments 1) and 2) in the enumeration are now shown more clearly in the manuscript and supported by the addition of the Figure 2a showing the attracting line coming from the Lee flow dividing R_1 and R_2. The inclusion of elliptic structures demonstrates core formation, and the core is defined earlier in the manuscript at the end of Section 2.

Technical corrections/ Editorial recommendations: pg 1, line 2: of > or

We have made the correction.

pg 2, line 33; kinematic structures as consequence of invertibility of vorticity: I cannot follow this argument. Please clarify.

We have clarified the statement to indicate that non-AEW disturbances provide no distinguished frame of reference.

pg 3, line 2; 'arm of T.S. Lee': incomprehensible

We have replaced 'arm' with the 'curved vorticity filaments emanating from' Lee.

pg 3, line 5: should read 'for a non-AEW disturbance'.

We have made the correction.

pg 3, line 12; suggest: initiated > first identified

We have made the suggested correction.

pg 5: should 'vortex strip' read 'vorticity strip'?

We have made the suggested correction.

pg 5, line 20: according to the references it should read 'Rutherford and Dunkerton, 2017.'

We have corrected the reference.

pg 6, line 4: This sentence seems to lack something, maybe 'vorticity' after 'system'?

We have changed the wording to 'system circulation' .

pg 6, line 5; 'isobaric vorticity substance' is non-standard terminology, possibly in analogy to the misnomer of 'isentropic potential vorticity'? Please clarify.

We have changed the wording to 'isobaric absolute vorticity'.

pg 6, line 14ff: This is an important paragraph, as it introduces the role of elliptic Lagrangian structures. As is, however, it is unclear how this paragraph links to the rest of the discussion at this point in the manuscript. I recommend including a similar discussion in the introduction.

We have added a definition of elliptic structures earlier in the paper which includes the Lagrangian vorticity.

pg 7; LCS: This and several other acronyms are not defined. The concept of a LCS (Lagrangian coherent structure) is not introduced either.

We have added the meaning of the acronym LCS and an explanation of what an LCS is. We have also clearly defined all other acronyms used in the paper.

pg 8; Lagrangian flow: unclear

We have changed 'Lagrangian flow' to 'Lagrangian manifolds'.

pg 9: It would be very helpful to mark R1 and R2 in the figure. In general, I find the idea to follow circulation areas and their merging in a Lagrangian sense quite interesting. With the current presentation, however, the discussion does not provide much insight to the reader.

The new Figure 2a showing the potential vorticity from Lee also shows the regions R_1 and R_2 and the curve that separates them, so that it is clear what regions the circulation values refer to.

pg 9, line 15ff: I cannot follow the role of Lee described in this paragraph.

The revised manuscript includes a new Figure 2a demonstrating the regions of high potential vorticity that originated from Lee, and this paragraph has been edited to point the reader to the key features in the figure.

pg 9, line 29, 30; comment on Lagrangian conservation of vorticity. Why should vorticity be conserved materially?

We have changed the wording so that this sentence could not be interpreted to mean that models other than the ECMWF model conserve vorticity.

pg 10, lobe transport of vorticity: It would be quite helpful for the reader to actually show figures including vorticity.

A figure showing the potential vorticity from Lee has been added in Figure 2a, and Figures 4 and 6 now show vorticity from the WRF simulations.

pg 14, line 8-9. Is the difference between 0.48 and 0.44 significant?

We have changed this section to reflect the analysis on the $\eta = 0.7$ level. The values of area reduction have been changed to reflect the new results, and the new text indicates that the difference between the two simulations is small.

Author's responses to review by Anonymous Referee #3 for "The genesis of Hurricane Nate and its interaction with a nearby environment of very dry air"

The authors would like to thank the reviewer for the detailed comments that we have used to improve the quality of this paper. We have written a new version of the manuscript that takes all of these comments into consideration. The responses to each of the individual comments is given below. The reviewer's comments are given below in italic while the author's responses are given in standard font.

In my opinion, this paper does not achieve its goal in illustrating how Nate interacts with its environment. Many results seem to be highly dependent on the way there are obtained and some statements are incorrect. It needs a major revision. First, all the paper is based on the role of the air mass that comes from storm Lee. However, no figure is given to show the evolution and decay of this cyclone. In addition, there is no precise definition of the air constituting Lee, and it is then difficult to see which air mass will be involved in Nate development. Second, the invariant manifolds may be highly sensitive on the way there are computed. From the different figures presented in the manuscript, small-scale motions may be very intense so as the exact position of the manifolds may change very much. Now, my more precise comments.

We thank the reviewer for the detailed comments and we have revised the manuscript that considers all of the reviewer's comments. We have made substantial revisions to the paper that strengthen the results and have corrected the errors. In particular, we have added Figure 2a showing the potential vorticity from Lee and the Lagrangian boundaries associated with the transport of this high potential vorticity air into the Nate development region, a precise definition of the region containing high potential vorticity from Lee, and the subsequent formation of the boundary associated with the sharp moisture gradient to the north of the Nate vortex. While the manifolds are sensitive to the way they are computed, e.g. due to the choice of the time interval used for integration, the sensitivity affects filaments that have little circulation, but does not affect the larger scale transport, so our major conclusions hold regardless of small scale uncertainties. We have added more precise statements about how the manifolds are computed, and have added an additional discussion about the sensitivity in Section 4.

1) Line 31, page 2.The definition of invariant manifolds based on a moving reference frame is wrong. Following your definition, any Galilean transform (e.g. rigid-body rotation) will change the position of saddle points and of the manifolds. The second definition given page 4 which relies on the Okubo-Weiss criterion is wrong as well, for the same reasons (see Lapeyre et al. Physics of Fluids 1999, Lapeyre et al. Chaos, 2001, Koh and Legras Chaos 2002, Haller JFM 2005). In the same manner, the authors cannot say page 14 that Okubo-Weiss is Galilean invariant! A correct definition of manifolds is given in the method section page 7.

We find this comment to be a misinterpretation of our definition on page 2, as the Lagrangian manifolds used in the analysis of Nate are not defined to be those of a stagnation point in the moving frame as clearly, the manifolds only coincide with Eulerian streamlines if one can assume that the flow and reference frame are steady. We have modified the text on page 4 to make it clear that a distinguished frame is still assumed at this point. The assumption of a steady flow in a moving frame of reference used in the definitions on page 2 and 4 are not used in any of the results in this study, and only serve as a motivation for the use of the correct definition on page 7. We have changed the wording on pages 2 and 4 to indicate that these manifold definitions are only valid in the case of steady flows where the frame is specified. The wording on page 14 for the Okubo-Weiss criterion has been changed to 'translation invariant'.

2) It is quite difficult to follow the paper as one needs to understand the different air masses origin and and there is no synoptic view of Lee (add a figure, please!) and a definition of its air mass. Also, can the author show Nate in its embedded environment (i.e. in a much larger spatial region)? An example of my difficulty in reading the paper is given page 3, lines 13-14 *when the authors state that "One or more vorticity filaments...". It would be very useful to see them! Same thing, about the S-shape (line 17). Can the authors illustrate the remnant air from Lee!*

The new Figure 2a showing Lee and the pre-Nate region demonstrates the interaction of these different air masses. The vorticity filaments and s-curve connecting the Nate and Lee flows that are described in the paper are now shown in the figure.

3) The discussion about the role of the Lee air mass in the genesis of Nate relies on the description of manifolds on isobar p=700hPa. However, Figs. 4, 5, 10 show that interpretations are highly sensitive to different parameters (altitude, divergence of the flow, SST...). Moreover, vertical motions are not included in the computation of the manifolds. It would be important to include these motions to see how the manifolds are dependent on this parameter as well. From what I see from the different figures, it is not clear to me that the positions in space of the manifolds are well defined. The very filamentary lobes may only exist because of advection by very small scales or errors in the velocity field. Manifold analysis is a powerful tool when the large-scale velocity fields is responsible of chaotic advection. Here, a lot of inertio-gravity waves seem to be emitted during convection and I wonder if they are quite energetic in terms of horizontal flow. If it is the case, that challenges a lot the interpretations of the paper.

We agree that the manifold filaments are sensitive to integration time, vertical level, divergence, SSTs, moist processes, or inertio-gravity waves. The contents of these filaments may also be quickly diffused, particularly when entrained into the core. While we show these filaments, the discussion in this paper is concentrated on the entrainment of the lobes from the dry air region which is not sensitive, as it appears in both ECMWF and WRF, with constant and varying SSTs, and aligns very closely with isolines of O_3. Thus, the key structures that we highlight are driven primarily by the large-scale velocity field, and only the filamentary regions, which have very little circulation, are strongly influenced by the small scales. A comparison of Figure 4 and 6 shows very similar manifolds even under separate model simulations. We have further explored the role of vertical motions by computing the manifolds in isentropic coordinates, and the same conclusions hold, even though the filamentary details are again different. The comparison of the non-divergent flow in Figure 5 to Figures 4 and 6 should not be seen as a sensitivity analysis but rather the demonstration of a dynamic process, since the non-divergent manifolds were created using only the non-divergent part of the velocity field, and not by turning off divergence in the WRF model. To clarify this issue, the new manuscript includes further discussion on the verification of robustness of large-scale Lagrangian structures. Specifically, we have added a paragraph of text when introducing O_3 and also in the Conclusions.

4) Page 9, second paragraph. What is the true definition of air coming from Lee? PV>some constant value ? air coming from latitude > 30 ? relative humidity < 50% ?

The air coming from Lee is that coming from above the attracting LCS within the pouch that is shown in the new Figure 2 (a) in the region labeled R_1.

5) Panels in Figure 3 are unreadable. The color scale for PV does not highlight low and high values; also it is not possible to discriminate positive and negative values in OW criterion.

We have changed the text color where needed to make the figures more readable, and have changed the color scale on the PV and OW plots to highlight low and high values.

6) How are precisely defined R_1 and R_2? This is important to follow the interpretation.

R_1 and R_2 are precisely defined by closed Lagrangian loops comprised of specific manifold segments terminating at specific endpoints and the regions are separated by an attracting boundary between them shown as a yellow curve in the new Figure 2 (a). The circulation values of these regions are precise because of the exact locations of the Lagrangian curves bounding them.

7) The authors give average values of relative vorticity. However there are two subtleties. First, there is some uncertainty in the exact area of the lobes. This should be quantified. Second, there are a lot of gravity waves and I guess there are local spots with high values of vorticity. This can strongly affect the average value, so that the average would be meaningless.

While there may be uncertainty in the manifold locations due to the spatio-temporal resolution of velocities, there is almost no uncertainty in the area of lobes or of the circulation since both the area and circulation are computed by a contour integral along the manifold using Green's Theorem. Mean vorticity is then computed as the ratio of circulation and area. Of course, the vorticity distribution is not constant, but the mean vorticity or circulation is a common and meaningful diagnostic of tropical cyclone strength.

8) Page 13. you should compare manifolds computed from trajectories along eta=0.6 and along p=600hPa surfaces to assess uncertainties in the position of the manifolds in the WRF simulation.

We now show the ECMWF at 700 hPa and WRF simulation at $\eta = .7$ for our primary analysis so that a more meaningful comparison between the ECMWF and WRF data can be made.

9) Figure 3 and 4 do not correspond to the same domain and the longitude axis is labelled differently. Please modify accordingly.

We have modified the figures so that the WRF and ECMWF plots show the same domain.

10) Page 13, line 18. "the flow on isobaric surfaces". I thought that it was on eta=0.6???

We have changed the text to indicate that the flow is on the eta=.7 level, where the new analysis is performed to make the WRF and ECMWF analysis more consistent.

11) I don't see the point to the paragraph about SST sensitivity. It does not seem to me that this paragraph is important for the discussion.

The forecast discussions for Nate indicate that actual intensity was lower than forecast intensity. Environmental interaction and lower SSTs from upwelling were given as possible causes for the lower intensity, and the paragraph about SST sensitivity shows the impact of lower SSTs in the WRF model. We demonstrate that the SST difference has little impact on the manifold configurations and only a modest impact on the strength of the vortex. The SST sensitivity paragraph has been revised to make the importance of this simulation more apparent.

12) I do not agree with the discussion on the the vortex radial structure. First, how do you define an "average" radial profile? The vortex is not axisymetric at all. How is defined its center? From Figure 3, OW and PV are quite noisy due to convection, so radial average may be meaningless. I thus do not understand what is plotted in Fig.8. Second, your definition of u and v is awkward. From the definition of T, we have $T(u,v) = (u,v)$ with $T = (u,n)/|u|$ Then $T(u,v) = (uu, -vvv, uv + uv)$ Hence $u = |u|$ and $v = 0$ So I don't see why the use of u would be interesting.

While the vortex is not axisymmetric, the flow near center is nearly circular so that radial profiles for small radii are meaningful. The center location is unambiguous as there is almost no difference between the locations from the best-track data set and the MRG pouch products, which were computed independently. The transformation matrix T orients the velocity field to give the tangent and normal components, thus $\tilde{u} = |\mathbf{u}|$ and $\tilde{v} = 0$. However, T is used to project derivatives of the velocities onto the tangent and normal directions, providing a 'natural coordinate' definition of normal strain and shear strain. We have made this more clear in the revised manuscript.

13) What are the uncertainties on the curves in Fig 7.

The curves in Figure 7 show the circulation interior to the manifolds, and the circulation is taken as a line integral along the curve, which has point spacing <=.01 degrees. There is no visible variation in the curves using a larger point tolerance. Any uncertainty in the circulation would be based on the location of the manifolds, and this sensitivity is discussed further in the conclusions, as indicated by our response to a previous concern.

14) Page 14,Line 21, the phrasing "vorticity moves inward" is misleading as it is not a 2D nondivergent transport. Also, it seems that the pouch boundary is defined through the OW criterion, which is quite different from the invariant manifold. Please clarify.

The flow near the center is not 2D non-divergent transport as upward mass flux causes convergence toward center, and we have changed the wording of this statement to indicate that vorticity increases toward the center due to convergence. The pouch boundary is defined through the invariant manifold locations, and not by the OW criterion, and the wording has been changed to make this point more clear. High OW is a characteristic of the core, and negative OW is characteristic of the shear sheath, not of the pouch boundary.

15) Panels of Fig. 10 should be at the same times as the Fig.2 Also, red/magenta colors are reversed with Fig.2

We have changed the colors on Figures 1 and 10 and times on Figure 10 to match those in Figure 2 so that the manifold colors are the same on all figures.

16) Conclusions. The fact that air cannot penetrate the vortex core while it can enter the pouch was discussed by Lapeyre Chaos 2002 and Babiano et al. Physics of Fluids 1994.

We have added a discussion including the results of these studies and references at the point in the paper where the vortex core is first defined in Section 2.

Abstract. The interaction of a tropical disturbance with its environment is thought to play an important role in whether a disturbance will develop or not. Most developing disturbances are somewhat protected from the intrusion of environmental dry air at mid-levels. For African easterly wave (AEW) disturbances, the protective boundary is approximated by closed streamlines in the wave-relative frame, and their interior is called the wave-pouch. The dynamic and thermodynamic processes of spin-up occur inside the pouch.

In this study we define the kinematic boundaries for a non-AEW disturbance in the Bay of Campeche that originated along a sharp frontal boundary in a confluent region of low pressure. We examine these boundaries during the genesis of Hurricane Nate (2011) to show how a pouch boundary on isobaric levels in the Lagrangian frame may allow for some transport into the pouch along the frontal boundary while still protecting the innermost development region. This result illustrates a generic property of weakly unsteady flows, including the time-dependent critical-layer of AEWs, that lateral exchange of air occurs along a segment of the boundary formed by the instantaneous, closed translating streamlines.

Transport in the Lagrangian frame is simplest when measured with respect to the stable and unstable manifolds of a hyperbolic trajectory, which are topologically invariant. In this framework, an exact analysis of vorticity transport identifies the primary source as the advection of vorticity through the entrainment and expulsion of bounded material regions called lobes. We also show how these Lagrangian boundaries impact the concentration of moisture, influence convection, and contribute to the pouch vertical structure.

1 Introduction

a. The cyclogenesis problem

The question of development versus non-development of tropical disturbances is a complex problem that has seen significant interest yet has an inherently high amount of unpredictability. There are many known factors that influence development, such as sea-surface temperatures, available moisture and vorticity, vertical wind shear, and the timing and distribution of convection, see e.g. Gray (1968) and McBride and Zehr (1981). Additionally, synoptic flow features often facilitate development by creating a favourable kinematic and thermodynamic environment where amplification of cyclonic vorticity can occur.

As seen by Frank (1970), most Atlantic tropical cyclones form along an African easterly wave (AEW). Along the wave trough, cyclonic vorticity is amplified by intense convection. The marsupial paradigm predicts the location for genesis to occur at the intersection of the wave-trough axis and wave critical layer where mean flow and wave phase speeds are equal (Dunkerton et al. (2009), hereafter DMW09). In the wave-relative frame of reference, a region of closed circulation, called the pouch, protects the embryonic vortex from adverse environmental conditions and the lateral intrusion of dry air and vertical wind shear. Inside the pouch, air is repeatedly moistened by convection while the parent wave is enhanced by diabatically amplified meso-scale eddies within the wave.

It is at the pouch boundary that the interaction of the proto-vortex with its environment occurs, and transport of any air across the boundary alters the physics within the pouch. When mixed into a vortex, dry air may quench convection reducing the total latent heat release and subsequent convergence, thus reducing the rate of or preventing spin-up of the vortex, see Kilroy and

Smith (2013). The role of this dry air and to what extent it is important are still relatively poorly understood due to the fact that entrainment and the definitions of the boundaries themselves are not well defined. In this study, we attempt to define the boundaries more rigorously so that the physical interactions between the pouch and environment can be better studied.

Permeability of the pouch boundary allows environmental air to enter a disturbance, which may prevent development if enough dry air reaches the circulation center, as was shown for Gaston (2010) by Rutherford and Montgomery (2012) and Freismuth (2016), a named tropical storm which was inhibited by dry air and vertical wind shear. Davis and Ahijevych (2012) and Montgomery et al. (2012) found that the pouch became increasingly shallower as the dry air intruded. However, Braun et al. (2012) found that if dry air is only partially entrained and does not reach the center, development may still occur, though the rate of intensification may be reduced.

A pouch whose boundary is open to transport on one side may also favor development, as Lussier et al. (2015) showed in the genesis of Hurricane Sandy (2012), if relatively moist environmental air is entrained into the pouch. In that paper it was shown that the pre-Sandy disturbance in the Caribbean was contiguous to the South American Convergence Zone (SACZ) on its equatorward side, and a direct kinematic pathway existed prior to storm formation, tapping the mid-level moisture of the SACZ. Fortunately for development, the pouch boundary was well-defined and closed on the northern side, sheltering from dry exterior air.

In AEW flows, the pouch boundary enclosing a region of recirculation can be seen by assuming a steady flow in the co-moving frame of the parent wave[1] with $\hat{\mathbf{u}} = \mathbf{u} - \mathbf{c}$ as in DMW09. In this frame, hyperbolic stagnation points $\mathbf{x}_{sp}$ satisfying $\hat{\mathbf{u}}(\mathbf{x_{sp}}) = 0$ appear along the wave's critical layer. The streamlines emanating from the stagnation points in the direction of the eigenvector of the negative/positive eigenvalue of the velocity Jacobian are called the stable and unstable manifolds, see e.g. Ottino (1990), and delineate the inner recirculating flow and open flow of the environment. In contrast to disturbances where the AEW provides the distinguished reference frame and antecedent kinematic structure, disturbances not originating from an AEW or other monochromatic tropical wave pathway do not have a distinguished frame of reference in which kinematic boundaries can be properly defined. These situations can be more complex, involving a combination of different disturbance types, possibly moving in different directions. In Nate (2011), a quasi-stationary tip rollup occurred at the SW end of a vorticity strip stretching across the Gulf of Mexico to connect with spiral bands emanating from the southwest of Tropical Storm Lee (2011), a storm moving eastward at the time. AEW flows are also more closely approximated by a 2D representation on a constant pressure level, while non-AEW flows may have a more significant vertical component in cases where baroclinicity is important.

In this study, we consider the kinematic boundaries and their impermeability with respect to advection on constant pressure levels and three-dimensional non-advective fluxes for non-AEW disturbances that form along a frontal boundary. We show that the boundary limits the advection of environmental dry air to that contained within a single closed material region plus non-advective fluxes, those fluxes not proportional to horizontal velocities, along the boundary. We depart from the wave critical layer theory and its associated translating critical points and manifolds for two reasons. First, there is no distinguished frame

[1]or moving with the feature associated with the large-scale flow when a wave is not present

of reference provided by the AEW, and second, the time-dependence of the flow causes trajectory paths to cross Eulerian streamlines in any translating or rotating frame.

b. Hurricane Nate (2011)

A surface low formed along a frontal boundary in the Bay of Campeche on Sept. 6 and the National Hurricane Center classified this disturbance as a tropical storm on Sept. 7. The pre-Nate pouch was first identified by the Montgomery Research Group on Sept. 6 as P25L[2]. One or more vorticity filaments extending across the Gulf of Mexico from the predecessor, Tropical Storm Lee, connected to Nate's region of formation. These filaments were associated with a strong horizontal gradient of water vapor orthogonal to the frontal boundary. An obvious question arises as to whether the "anti-fuel" behind the frontal zone would affect Nate adversely, or if no adverse effects ultimately were seen, why not? During the development of Nate, the frontal zone itself was deformed into a graceful S-curve by the combined action of Lee and Nate at opposite ends of the frontal zone.

Over the next few days, dry air to the north of the frontal boundary, with ECMWF relative humidity values less than 20% throughout the mid-troposphere, was in close proximity to Nate, yet Nate was still able to intensify. Since satellite visible imagery indicated that dry air remained approximately 1 degree from the storm center, we question whether, and to what extent, environmental dry air reached the core. Factors helping the development of Nate included sea surface temperatures (SST)[3] greater than 29 C and little vertical wind shear. After strengthening briefly to hurricane status for 6-12 hours on Sept. 8[4], Nate weakened to a tropical storm on Sept. 9 after showing mid-level dry air and cooler ocean temperatures (SST$<$27 C) presumably from up-welling created by the stationary storm. After Nate began to track westward, it briefly began to intensify on Sept. 10 before making landfall as a tropical storm in central Mexico on Sept. 11. A summary of Nate is given in Avila and Stewart (2013).

In this study, we examine the 2D Lagrangian flow structures on isobaric surfaces from ECMWF model analyses to describe the transport of dry air and evolution of vorticity at mid-levels. The Lagrangian manifolds defined in the upcoming section indicate what flow features, including the remnants of Tropical Storm Lee, contributed to the circulation of Nate and measure the impact of dry air that Nate interacted with after genesis. The Lagrangian boundaries are also shown in relation to regions of convection to show that convection is typically located interior to Lagrangian boundaries.

c. Outline

The outline of the remainder of this paper is as follows. Section 2 provides an introduction to the mathematical methods for the location of Lagrangian boundaries. In Section 3, we show numerical details of the computations and data sets. In Section 4, we describe the genesis of Nate from the perspective of the evolution of Lagrangian manifolds. In Section 5 we provide a detailed description of the interaction of Nate with its environment, and show how the Lagrangian flow boundaries offer both

---

[2]The pre-Nate pouch was called P25L as the 25th pouch of the 2011 Atlantic season. This name is used to show the location of the storm for the remainder of this paper.

[3]Sea surface temperature data is from the NCDC Optimum Interpolation Sea Surface Temperature (OISST) .25 degree resolution data set

[4]http://weather.unisys.com/hurricane/atlantic/2011/NATE/track.dat

protection from the outer environment, and help to concentrate vorticity into the vortex core. Conclusions and a discussion of future work are provided in Section 6.

2 A review of stable and unstable manifolds of a hyperbolic trajectory and lobe transport

In generic time-dependent flows in a distinguished frame of reference, flow boundaries are a set of distinguished material curves called the stable and unstable manifolds of a hyperbolic trajectory, see e.g. Ottino (1990) and Samelson and Wiggins (2006). Trajectories of the flow satisfy

$$\dot{\mathbf{x}} = \mathbf{u}(\mathbf{x}, t), \tag{1}$$

where $\mathbf{u} = (u, v)^T$ is the fluid velocity and $\mathbf{x} = (x, y)^T$ is the Earth-relative particle location. At instantaneous snapshots, the stability of an air parcel is determined by the eigenvalues of its linearized velocity field. The Okubo-Weiss parameter (OW) accounts for shear and strain to distinguish solid-body rotation from parallel shear flow or stretching regions. Imaginary eigenvalues (or complex conjugate pairs when horizontal divergence is non-zero) of $\nabla \mathbf{u}$, indicate elliptic stability or rotation-dominated flow, and occur when $OW = \frac{1}{4}(\zeta^2 - S_1^2 - S_2^2) > 0$ where relative vertical vorticity is $\zeta = v_x - u_y$, and $S_1 = u_x - v_y$ and $S_2 = v_x + u_y$ are the strain rates. Hyperbolicity is marked by real eigenvalues of opposite signs of the velocity Jacobian, i.e. $OW < 0$. A hyperbolic trajectory $\mathbf{x}_h(t)$ is a trajectory that remains hyperbolic for all t. The stable and unstable manifolds manifolds of $\mathbf{x}_h(t)$ are its attracting sets forward and backward in time,

$$S(\mathbf{x}_h(t)) = \{\mathbf{x} : \mathbf{x}(t) \to \mathbf{x}_h(t), t \to \infty\} \tag{2}$$

$$U(\mathbf{x}_h(t)) = \{\mathbf{x} : \mathbf{x}(t) \to \mathbf{x}_h(t), t \to -\infty\} \tag{3}$$

A hyperbolic trajectory has local subspaces, $S_{loc}(\mathbf{x}_h(t))$ and $U_{loc}(\mathbf{x}_h(t))$ that are tangent to the eigenvectors of the negative/positive eigenvalue of the Jacobian. Therefore, the stable and unstable manifolds are the material curves which are initially $U_{loc}(\mathbf{x}_h(t))$ and $S_{loc}(\mathbf{x}_h(t))$, and can be computed by the advection of the local initial segments. The hyperbolic trajectory may be located near an Eulerian saddle chosen in a proper reference frame, leading to numerical algorithms for their location, see Ide et al. (2002) and Mancho et al. (2003). In forward time, particles along hyperbolae adjacent to the stable/unstable manifolds are repelled/attracted to these manifolds. The attracting property of the unstable manifold leads to intense gradients of active and passive scalar tracers, a prominent feature in the atmospheric case examined here.

Due to the difference in the direction of time in the stable and unstable cases, the manifolds may cross at points other than hyperbolic stagnation points, forming material regions, called lobes, that are enclosed by multiple manifold segments. The time-evolution of lobes describes the transport of material “across" the Eulerian boundary and is called lobe dynamics, see Wiggins (2005), Duan and Wiggins (1996), Malhotra and Wiggins (1998). The equivalent term “lobe transport" is introduced by Wiggins (2005) and highlights the role of lobes in altering the distribution of active and passive scalars in geophysical flows. Hyperbolic trajectories, their stable and unstable manifolds, and lobe transport have been applied to many geophysical flows, including Koh and Plumb (2000), Joseph and Legras (2002), Rogerson et al. (1999), Miller et al. (1997), Branicki et al. (2011), Mancho et al. (2006b), Malhotra and Wiggins (1998), Wiggins and Ottino (2004), Duan and Wiggins (1996), Koh and Legras (2002), Wiggins (1992), Rom-Kedar et al. (1990). Lobe transport has also been applied by Rodrigue and Eschenazi (2010) to flows with similar flow boundaries as those in pre-genesis cases, including a Kelvin-Stuart cat's eye flow. In tropical cyclones, lobe dynamics allows one to quantify the net entrainment of relatively dry (and hence low entropy) air, the so-called “anti-fuel" of the hurricane problem.

Boundaries of physically important regions in time-dependent flows may be formed by connected stable and unstable manifold segments that form an enclosure called a separatrix[5]. As the flow evolves with time, the separatrix is redefined as a different set of manifold segments at a later time so that it remains most similar to the expected physical boundary, see e.g. Rom-Kedar et al. (1990).

In the case of Rossby-wave critical-layer flows, a cat's eye region of recirculation is expected (Benney and Bergeron, 1969), which governs not only the kinematics but also the dynamical redistribution of vorticity within the cat's eye and simultaneous reflection or over-reflection of incident Rossby waves (Killworth and McIntyre, 1985). In such cases, the “expected physical boundary" corresponds to the separatrix surrounding the cat's eye. A suitable generalization for unstable Rossby waves on a vortex strip is to imagine that the separatrix becomes wider with time, prior to the emergence of distinct gyres and possible vortex pairing (Rutherford and Dunkerton, 2017). While it is beyond our immediate scope to identify an expected physical boundary in the formation of Nate (2011) along its antecedent vortex strip, our analysis of manifolds suggests unequivocally that such a physical boundary exists.

A schematic of the time-evolution of manifolds of hyperbolic trajectories H_1 and H_2 in a cat's eye is shown in Figure 1 at times t_1 (a) and t_2 (b). The stable manifolds S_1 and S_2 are shown in magenta and red while the unstable manifolds U_1 and U_2 are shown in blue and cyan. The intersection points of stable and unstable manifolds at points other than H_1 and H_2 are labeled I_k for $k = 1$ to $k = 6$. The separatrix for the time-dependent cat's eye flow is the combination of stable and unstable manifold segments that most represent an Eulerian cat's eye, and is defined at t_1 as $V(t_1) = U_1(H_1, I_1) \cup S_2(I_1, H_2) \cup U_2(H_2, I_6) \cup S_1(I_6, H_1)$. By time t_2, the separatrix is defined as $V(t_2) = U_1(H_1, I_3) \cup S_2(I_3, H_2) \cup U_2(H_2, I_4) \cup S_1(I_4, H_1)$ to maintain a cat's eye shape. The lobes labeled L_1 and L_3 are transported from outside the separatrix to inside the separatrix and lobes L_2 and L_4 are transported from inside the separatrix to outside the separatrix.

The change in system circulation due to the advection of each lobe may be computed using Stokes' theorem along the lobe boundary. Haynes and McIntyre (1987) and Haynes and McIntyre (1990) find that as a consequence of the impermeability

[5]In idealized theoretical models of nonlinear critical-layer flows, the cat's eye boundary is a separatrix of total (wave + mean) stream function inside of which absolute vorticity is advected passively to leading order, see e.g. Killworth and McIntyre (1985); Samelson and Wiggins (2006), and references therein. Elsewhere we refer to this stream function geometry as a “wire-frame" induced by the superposition of wave and mean shear: that is, the result of wave propagation prior to nonlinear overturning of vorticity and passive scalars in the cat's eye (see Figure 1 of DMW09). Lagrangian manifold growth tends to parallel the existing wire-frame, as absolute vorticity is a dynamical tracer. This description is appreciated best in slowly varying flows. By the same token, lobe dynamics is most significant when fast but small background oscillations are superposed on the slower wave, mean-flow interaction. In rapid or highly transient developments, a crisp distinction of interior and exterior flows may not have time to materialize, in which case the vortex core is largely unprotected prior to shear sheath formation. In the absence of hostile influences, storm formation is possible without a separatrix, given enough time, but such simulated developments are unrealistic, as are the underlying assumptions of these spontaneous aggregation experiments.

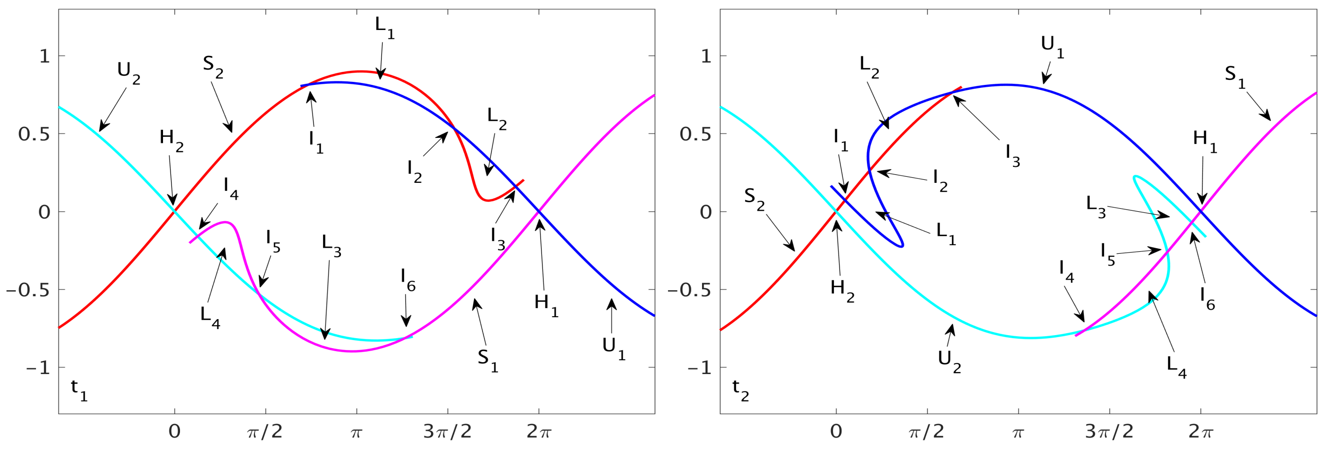

(a) (b)

Figure 1. Diagram of lobe transport for a time-dependent cat's eye flow where the contents of the lobes are transported across the separatrix boundary formed by the unstable (blue and cyan) and stable (red and magenta) manifolds of a pair of hyperbolic trajectories. The lobes labeled 'L_1' and 'L_3' begin outside the cat's eye and are transported to inside the cat's eye.

principle, isobaric vertical vorticity is conserved on isobaric surfaces, implying that the circulation within the pouch and lobes is conserved with respect to advective fluxes, and all changes to the pouch circulation from advection are due to lobe transport across the expected physical boundary surrounding the "pouch", so defined. Non-advective fluxes, or those not proportional to horizontal velocities resulting from tilting, friction, and sub grid-scale forces, may act across any material curve including the pouch boundary and across the lobe boundaries, see Haynes and McIntyre (1987).

Since the unstable manifold is attracting under a forward time integration, tracer-like quantities such as equivalent potential temperature (θ_e) and ozone tend to develop strong horizontal gradients along the unstable manifold. If moist convection is located interior to the unstable manifold in the region of confluence of θ_e, i.e. on the side of the manifold with higher θ_e, then these boundaries influence not only the two-dimensional vorticity aggregation, but also vorticity amplification through isobaric convergence caused by three-dimensional stretching in moist convection.

In their mature stage, tropical storms exhibit an additional inner pouch boundary as a Rankine-like vortex core with solid-body rotation is isolated from the pouch exterior by a ring of strong differential rotation (azimuthal shearing), see Rutherford et al. (2015). It is a quasi-circular region of intensely negative Lagrangian OW parameter in stark contrast to the positive OW vortex core, (Rutherford et al. (2015)). The "shear sheath", as we will call it, is effectively a boundary to particle transport and protects the vortex core from interaction with the environment, allowing the vortex to become self-sustaining. These shear sheaths and vortex cores have been observed in many geophysical flows, e.g. McWilliams (1984), Beron-Vera et al. (2010).

While the Lagrangian manifolds characterize the pouch as semi-permeable to transport, whether these intrusions disrupt the internal processes is determined by the existence of an additional boundary between the core and the cat's eye boundary called a shear sheath. In most developing disturbances, the region of high vorticity in the center behaves as a finite-time KAM torus, with little straining deformation, no mixing, and in solid-body rotation. Particles in the core act coherently as a vortex, meaning that they have the same Lagrangian averaged rotation rate, see Haller (2015). The vortex core is a convex set of the Lagrangian averaged vorticity field, defined as

$$\zeta_{Lag}(t_0,t) = \int_{\mathcal{I}} \zeta(\mathbf{x}(s))ds \tag{4}$$

where $\mathbf{x}(t)$ is the particle trajectory initialized at the point $(\mathbf{x_0},t_0)$ and trajectories are initialized as a grid and then advected using the two-dimensional velocity field over the time interval $\mathcal{I} = (t_0 - t_1, t_0 + t_2)$. The lack of mixing in the core is a well known fluid dynamical concept, having been observed in many flows even when there is permeability of the outer boundary, see e.g. Babiano et al. (1994); Lapeyre (2002). Outside of the KAM-torus or vortex core, a region of exceptionally high straining called the shear sheath provides protection to the core as a dynamical barrier with high vorticity gradient, and creates filaments chaotically of parcels that attempt to enter into it. Following Rutherford et al. (2015), the shear sheath can be seen as a minimal annulus of the Lagrangian OW field defined by

$$OW_{Lag} = imag(G) - real(G), \tag{5}$$

where G is formed by time-integrating the eigenvalue λ_+ of the velocity gradient tensor $\nabla\mathbf{u}$ along particle trajectories $\mathbf{x}(t)$,

$$G = \int_{\mathcal{I}} \lambda_+(\mathbf{x}(t),t)dt. \tag{6}$$

$\mathcal{I}$ is the time interval of interest, here a sliding 72 hour time interval, $\mathcal{I} = (t-36, t+36)$. Just as lobe dynamics was seen during genesis, a vortex core and shear sheath surrounding it are present just after genesis, and these structures define the Lagrangian topology once there has been significant folding near the hyperbolic trajectories.

3 Numerical methods and data

a. ECMWF model output

For this study, we use operational ECMWF model analyses constructed at the start of each assimilation cycle to initialize forecast models with velocities and thermodynamic variables given on a regular 0.25×0.25 degree grid every 6 hours.

To compare the ability of the ECMWF analyses to correctly represent the Lagrangian topology with 6 hour data, we also use WRF simulations at 10 km horizontal grid-spacing with 10 minute output intervals. The WRF simulations were initialized with 25 km ECMWF analyses. The ECMWF analyses were used to control the boundary conditions for the entire simulation.

b. Computation of fluid velocities and trajectories

Trajectory computations use isobaric velocities with bi-cubic interpolation in space and time. Manifold computations and Lagrangian scalar fields come from sets of particle trajectories, which are computed using a fourth order Runge-Kutta method with an intermediate time step of 15 minutes for the ECMWF trajectories and at the model output timestep of 10 minutes for the WRF simulations to accurately represent the curvature of particle paths.

c. Manifold computations

Manifolds in time-dependent flows require the location of a hyperbolic trajectory and its local stable and unstable manifold segments. The initial segment used to construct Lagrangian manifolds is typically a line segment that straddles a hyperbolic trajectory. Hyperbolic trajectories are difficult to locate prior to manifold computation since they require first identifying a distinguished frame of reference and then locating quasi-steady saddle points in that frame. Alternatively, material surfaces called Lagrangian coherent structures (LCSs) may still be found which strongly influence nearby trajectories. If LCSs can be located, manifold segments are initialized along attracting LCSs found in a forward direction in time for the unstable manifold segments and in a backward direction in time for the stable manifold segments. Ridges of the finite-time Lyapunov exponent (FTLE) field have been used for initial segment location for the polar vortex by Koh and Legras (2002). Such initial segments can, in fact, be relatively long compared to a typical initial segment, having acquired already the distended shape of an unstable manifold prior to further advection and distention after initialization. Here, we use the strainline approach of Farazmand and Haller (2012) for initial segment location, where local attracting manifold segments are found to be lines that contain a maxima of the greater eigenvalue of the Cauchy-Green deformation gradient tensor, and are everywhere tangent to the eigenvector field associated with the smaller eigenvalue. The Cauchy-Green deformation tensor is defined as $C = (\nabla F)^T(\nabla F)$ where $F = d\mathbf{x}/d\mathbf{x}_0$ is the Lagrangian deformation tensor and T is the matrix transpose. The tensors C and F have an integration time associated with them, which is relatively short compared to the entire time interval under which genesis occurs, chosen here as 24 hours forward from the initial time and 24 hours backward from the final time. Locating initial segments may also be done using Eulerian strainlines, as defined by Serra and Haller (2016). A choice of 24 hours was long enough to eliminate spurious Eulerian strainlines while limiting excessive filamentation of the initial segment. Once the manifolds are known, hyperbolic trajectories can be deduced as the intersection of the stable and unstable manifolds.

Manifolds are advected using the algorithms of Mancho et al. (2003) and Mancho et al. (2006a). As the manifolds are advected, the entire set of points evolves, and additional points are inserted when adjacent points grow too far apart. Lagrangian manifolds are advected for the finite time interval during which the hyperbolic trajectories are known to exist. The value of t is chosen at the *beginning* of a sliding time window for the *unstable* manifold (obtained from forward trajectories) and the *end* of the interval for the *stable* manifold (obtained from backward trajectories). This time interval is designed to optimize the description of Lagrangian manifolds of finite duration, and consists of fixed, discrete, non-overlapping windows (to highlight stages of development, as in this paper) or as overlapping windows that slide forward automatically in time (as in the Montgomery Research Group pouch products, when the stages of development are not yet identified in near real-time). The choice of start time and end time for manifold integration change the manifold length, as longer integration times produce longer manifolds and more lobes. Manifolds integrated for shorter times may not produce a closed separatrix or lobes. Our choice of integration time is driven by the objective of capturing the entrainment of the dry air while minimizing the number of additional lobes.

4 Genesis of Nate

Tropical Storm Lee left the Gulf of Mexico on 3 Sept., making landfall in Louisiana and traveling northeast. From 4 Sept. to 6 Sept., southerly flow in the Gulf of Mexico guided moisture and remnant vorticity from Lee into the Bay of Campeche where a frontal boundary between moist air to the south and very dry air to the northeast was established. The potential vorticity field showing the pre-Nate region and TS Lee is shown at 0 UTC 6 Sept. in Figure 2 (a). This moisture and vorticity accumulated in a confluent region of low pressure in the southern Gulf of Mexico. Over the next day, the area of low pressure became better organized and showed curved banding features, increased convection, and a well-defined low-level circulation, prompting NHC to initiate the system as Tropical Storm Nate at 2100 UTC 7 Sept., with a conservative 40 kt wind speed estimate taken from oil rig and aircraft measurements[6].

In the nearly stationary frame of the 700 hPa Nate flow in ECMWF model analyses, there was no pouch at any level on 5 Sept. However, there is a saddle point visible on 4 Sept. at 500 hPa in the frame of reference moving with Tropical Storm Lee to the north at $c_y = 5$ m/s (not shown). The saddle point in the nearly stationary frame of Nate emerges at progressively lower levels, emerging at 700 hPa at 1200 UTC 6 Sept., and its streamlines form an enclosed Eulerian pouch at 0 UTC 7 Sept.

a. Manifolds and lobe transport

We consider now the period of formation by analyzing the Lagrangian manifolds from 0 UTC Sept. 6 to 0 UTC Sept. 9 to see the sources of vorticity and the establishment of a pouch boundary as a barrier to very dry air. The manifolds are overlaid on the θ_e field at 700 hPa for this time period in Figure 2 (b)-(g). The manifolds and pouch region are labeled in (b), while the time evolution is shown at 12 hour snapshots in (b)-(g). The stable manifolds S_1 and S_2 are shown as magenta and red curves, respectively, while the unstable manifolds U_1 and U_2 are shown as blue and cyan curves, respectively. The initial segments of U_1 and U_2 were located as strainlines at 0 UTC Sept. 6 and were advected forward in time, while the initial segments of S_1 and S_2 were strainline segments from 0 UTC Sept. 9 that were advected backward in time. From the intersections of these manifolds, we can deduce the locations of two hyperbolic trajectories, labeled H_1 and H_2 in Figure 2 (b). H_1 is the intersection of U_1 (blue) and S_1 (magenta) at the northeast of the pouch, and H_2 is the intersection of U_2 (cyan) and S_2 (red) at the southwest of the pouch. These hyperbolic trajectories are in close proximity to a pair of Eulerian saddles (not shown) that emerge along the regions of confluence on 6 Sept. and are trackable until 10 Sept. There are additional intersection points between the manifolds as I_1 and I_2 mark the intersections of U_1 and S_2. Similarly, U_2 and S_1 intersect at I_4. As defined in the mathematical methods section, we can define the pouch as the interior of the connected curves $U_1(H_1, I_1) \cup S_2(I_1, H_2) \cup U_2(H_2, I_4) \cup S_1(I_4, H_1)$.

The unstable manifolds comprising the pouch boundary are attracting regions that can actually be observed before Sept. 6. On 5 Sept., there are two attracting lines in the confluent region from the Lee flow, one from the southern side and one from the northern side. The origin of U_1 is the attracting line from the northern side that is advected southward and becomes the obvious dry air boundary by Sept. 6. Additional attracting lines are advected southward from the Lee flow. Most importantly, one of these lines differentiates the region of the pouch interior that was advected from Lee versus the part that came from the

[6] National Hurricane Center Tropical Storm Nate Discussion Number 1. http://www.nhc.noaa.gov/archive/2011/al15/al152011.discus.001.shtml

Nate development region. The location of this line can be seen as the yellow curve in Figure 2 (a) that divides the pouch region into R_1 to the north of the yellow curve with origins from Lee and R_2 the portion of the pouch with southern Gulf of Mexico origins. The different properties of these regions can also be seen in the latitude tracer field in Figure 3 (a), which shows the initial latitude of trajectories advected backward 48 hours from the gridded locations at 18 UTC Sept. 6. The contents of the pouch at this time coming from Lee have initial latitudes of greater than 30 degrees, while the portion with Gulf of Mexico origins have latitudes less than 30 degrees. We see that the pouch region that originated from Lee still contains high potential vorticity air, Figure 3 (b). The difference between these regions is also clearly visible in the ozone mixing ratio, Figure 3 (e), where higher values are present in R_1. The third attracting curve is located over Mexico and the southern Gulf of Mexico, and becomes U_2, the southern boundary of Nate during the genesis period. The stable manifold segments S_1 and S_2 can be located on 0 UTC Sept. 9.

On 12 UTC Sept. 5, the area of R_1 is $1.5\times10^5 km^2$, while the area of R_2 is $2.8\times10^5 km^2$, with a total area of $4.3\times10^5 km^2$. As R_1 and R_2 are mixed, convergence causes a decrease in their areas to $1.3\times10^5 km^2$ and $2.3\times10^5 km^2$ for a combined area of $3.6\times10^5 km^2$. The circulation of R_1 is $3.4\times10^6 m^2/s$ at 12 UTC 5 Sept. and increases to $5.3\times10^6 m^2/s$ by 18 UTC 5 Sept. before steadily decreasing to $3\times10^6 m^2/s$ by 12 UTC 7 Sept.[7] The circulation of R_2 steadily increases from no circulation at 12 UTC 5 Sept. to $2.8\times10^6 m^2/s$ at 12 UTC 7 Sept. The combined circulation is $3.4\times10^6 m^2/s$ at 12 UTC 5 Sept. and increases to $5.8\times10^6 m^2/s$ by 12 UTC 7 Sept. At the time of genesis, 52% of the circulation of Nate comes from the region R_1 advected from Lee while the remainder is vorticity that was already present in the area of low pressure in the Bay of Campeche. The mean vorticity in R_1 reaches $5.2\times10^{-5}s^{-1}$ at 0 UTC 6 Sept. before declining to $2.7\times10^{-5}s^{-1}$ at 12 UTC 7 Sept. The mean vorticity of R_2 increases steadily to $2.8\times10^{-5}s^{-1}$ at 12 UTC 7 Sept. In the ECMWF numerical data, the horizontal advection of vorticity accounts for over half of the change in circulation while the remainder of the change in circulation is due to nonadvective fluxes of vorticity. Similarly, the non-advective flux contains unresolved advective fluxes. In principle, one might calculate the unresolved advective flux by subtracting the resolved non-advective flux from the residual of total tendency and advective flux.

The more complicated structure of the Lagrangian manifolds and their additional intersections allowed the formation of lobes. The lobe $L_1 = U_1(I_1, I_2)\cup S_2(I_2, I_1)$ is enclosed by U_1 and S_2, and is initially located to the north of Nate in the region of very dry air. Its advection can be seen in Figure 2 (b-g). Prior to development, the lobes did not penetrate into the center where regions of highest OW were located, Figure 3 (c). The intersection points I_1 and I_2 travel cyclonically around the boundary and by 0 UTC 9 Sept. the intersection points have traveled close to H_2, as L_1 has begun to be ingested into Nate. During the entrainment of L_1, the very small lobe $L_2 = U_1(I_2, I_3)\cup S_2(I_3, I_2)$ is expelled from the vortex. At this time, the northern boundary of the pouch is redefined from $U_1(H_1, I_1)\cup S_2(I_1, H_2)$ to $U_1(H_1, I_3)\cup S_2(I_3, H_2)$, which reflects the inclusion of the contents of L_1 into the pouch interior and expulsion of L_2. L_1 originated from the dry air region and transported the dry air toward the center. Though the development of Nate occurred on Sept. 7 before the dry air could reach the center, the dry air also contained lower vorticity than the moist air in the pouch, and reduced the mean vorticity within the pouch. By 0 UTC

[7] The non-advective isobaric absolute vorticity vector differs from the advective vector and therefore can cross material contours.

Sept. 8, L_1 had a negative relative circulation. Without the contents of L_1, the mean vorticity in the pouch was 3.1×10^{-5}, versus 1.8×10^{-5} when L_1 is included.

In addition to L_1 and L_2, there are additional lobes, $L_3 = U_2(I_4, I_5) \cup S_1(I_5, I_4)$ and $L_4 = U_2(I_5, I_6) \cup S_1(I_6, I_5)$, labeled in Figure 2 (b), that transport air across the southern pouch boundary. L_3, the interior of the region bounded by the cyan and magenta curves, contains moist air with high vorticity on the southern boundary of Nate, and travels inward transporting this air into Nate. L_4 contains a small amount of moist air with high vorticity that is initially in the interior of Nate, and over the three day time period, this air is expelled to the east through lobe transport. As the four lobes are transported, a rearrangement of the boundary occurs, and by 1800 UTC 8 Sept., Nate contains the contents of the pouch from 0 UTC 6 Sept. minus the contents of L_2 and L_4, but with the addition of L_1 and L_3, Figure 2 (g). Since L_2 and L_4 are relatively small, they have little effect on the circulation.

b. Relation of Lagrangian boundaries to tracers and convection

The Lagrangian boundaries are closely related to the transport of tracers as Lapeyre et al. (1999) found that the maximum tracer gradient tends to align with the unstable manifold. The relationship of the manifold boundaries to both physical, e.g. potential vorticity and ozone (O_3), and advected tracers can be seen in Figure 3. The potential vorticity and O_3 fields are shown at 700 hPa at 1800 UTC Sept. 6 in Figure 3 (b) and Figure 3 (e), respectively. The intrusion of dry air entering the northwest side of the pouch is visible in the θ_e and O_3 fields, with higher O_3 and lower PV air contained in L_1. The gradient of the θ_e field, Figure 2, indicates a strong frontal boundary between moist and dry air to the north of the pouch that aligns very closely with U_1. However, the ozone field acts as a better tracer than θ_e since its filaments more closely follow the filaments of the manifolds, and isolines of O_3, Figure 3 (e), still approximately separate the air with origins from Lee (see R_1 in Figure 2 (a)) from the air with southern Gulf of Mexico origins. Small differences between the tracer gradients and manifolds are due to the non-conservation of the tracers.

Advected tracers form steep gradients purely from advective transport and can be seen by plotting the initial value of the advected quantity at the final location of the particle. Behavior similar to that of the other physical tracers can be visualized by the latitude tracer field (conserving initial latitude along trajectories), which shows the initial latitude of particles (Figure 3 (a)). In each case, there is an obvious alignment of the unstable manifold with the sharpest gradient of the tracer field.

We examine now whether the accumulation of moisture and confluent flow along the unstable manifold impacts the location of convection. The 700 hPa stable and unstable manifolds are overlaid on GOES shortwave infrared 3.9 μm brightness temperature (K) averaged over a 6 hour time interval spanning 0 UTC in Figure 3 (d). By 1800 UTC Sept. 6 a significant amount of moderately cold clouds are evident along the frontal boundary south of the unstable manifold (U_1, blue) in the southwest quadrant of the storm. The manifold boundary clearly partitions the cloudy region from the less cloudy regions. Though the moisture gradients align with the manifold boundaries, as seen in the relative humidity field in Figure 3 (f), the azimuthal location of convection in relation to these boundaries is far less predictable, though it does tend to be on the interior of the boundary.

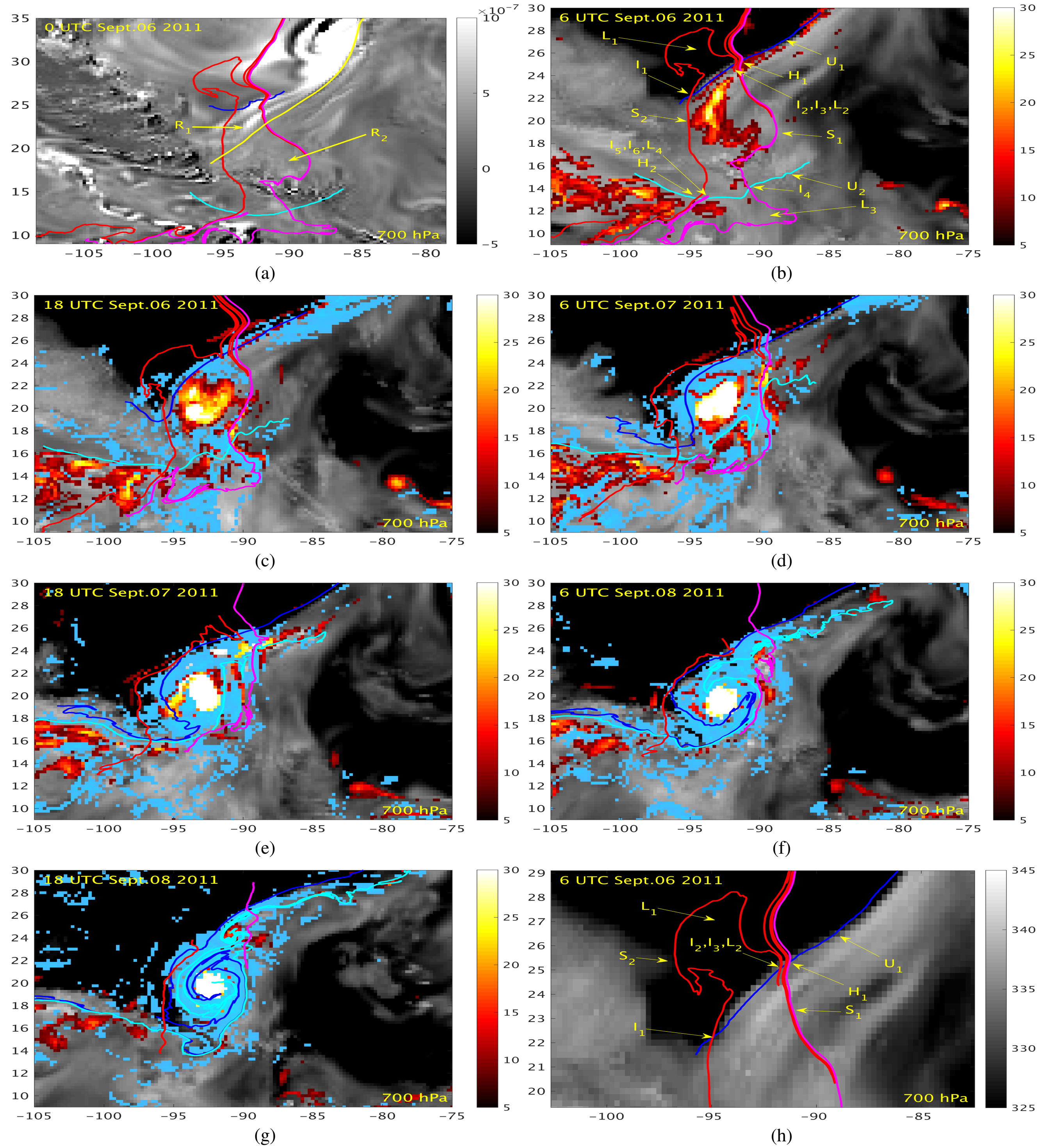

Figure 2. The stable (red, magenta) and unstable (blue, cyan) manifolds are overlaid on the ECMWF PV field $(M \cdot m^2/kg \cdot s)$ in (a) and θ_e field (K) (background with gray colors) at 700 hPa in (b-g) showing the time-evolution of the manifolds from Sept. 6 to Sept. 8. The hot colormap shows the ζ_{Lag} values while the cool colors indicate OW_{Lag} values of less than -8 indicating high strain. Labels are provided in panels (a) and (b). A zoom of the features that are shown in panel (b) is shown in panel (h), which also shows the colorbar for the θ_e field. An attracting line from the Lee flow is shown in yellow in (a).

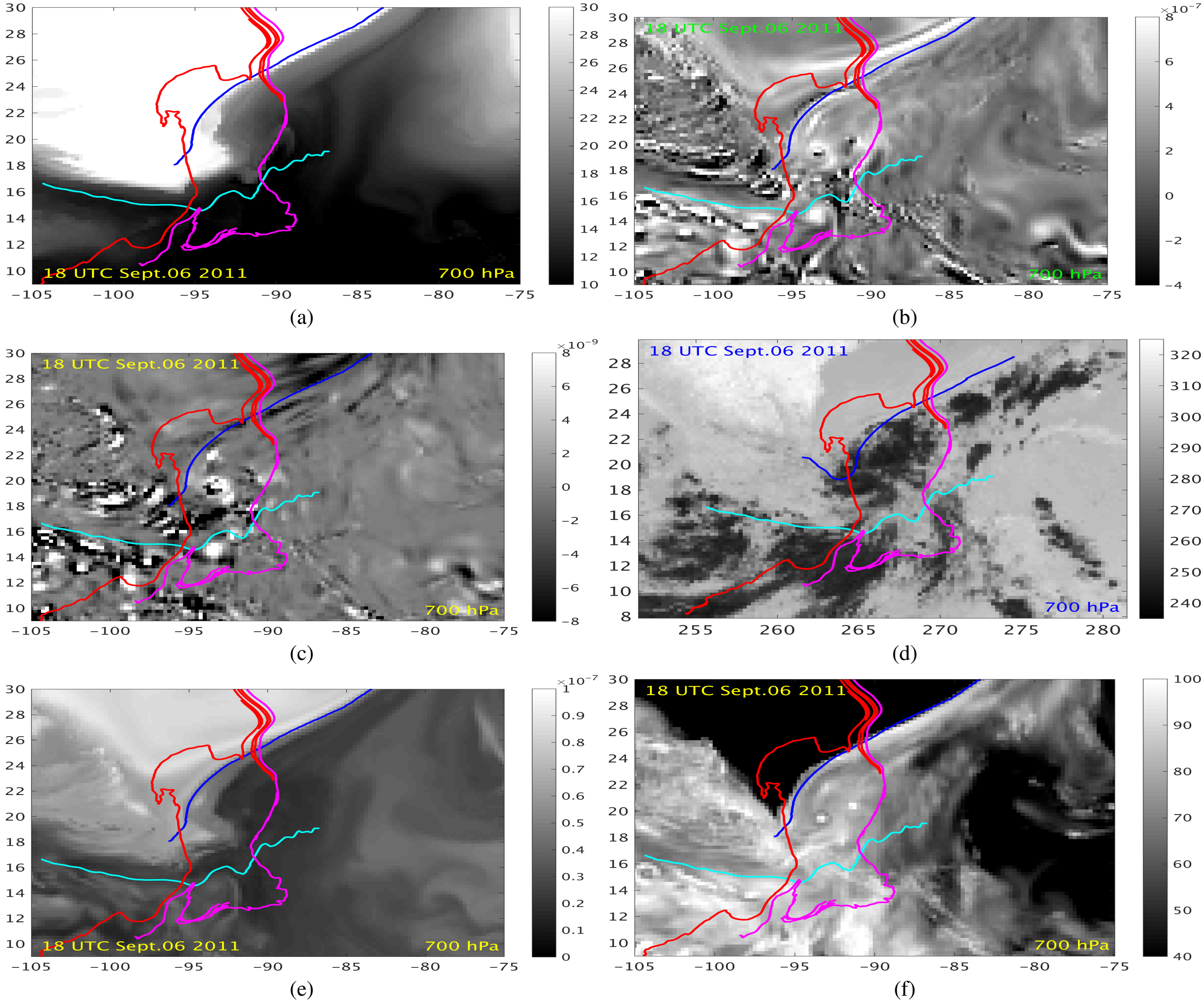

Figure 3. The stable (red, magenta) and unstable (blue, cyan) manifolds are overlaid on the latitude tracer field (degrees) in (a), the PV field $(K \cdot m^2/kg \cdot s)$ in (b), the OW field (s^{-2}) in (c), the GOES 3.9 μm brightness temperature (K) in (d), the ozone mixing ratio (g/kg) in (e), and the relative humidity field (f) at 18 UTC Sept. 6 at 700 hPa.

c. Lobe transport in the WRF model

The WRF model simulation is used to compare how temporal resolution, spatial resolution, divergence, and varying versus constant SSTs affect the manifold topology. Lobe transport is shown for the complimentary WRF simulation in Figure 4 where the Lagrangian manifolds are overlaid on the vorticity field at the model η-level of 0.7, or approximately 700 hPa. Though the fine structure is different, the topology that emerges from ECMWF analyses and WRF outputs are very similar on the northern side of the disturbance with a pair of hyperbolic trajectories. A single large lobe is present in the dry air region to the north, with similar structure and location as L_1 from the ECMWF model, while a smaller filamentary lobe begins in the pouch and is ejected. Similar lobe transport is present in the WRF simulation on the southern side as in the ECMWF analyses. As noted earlier, the ECMWF analyses at 6 hour time intervals is not sufficient to close the circulation budget over a 72 hour time interval as a large residual non-advective flux term remains. The advantage of the finer temporal resolution is that the circulation budget has advective and tilting fluxes that remain larger than residual non-advective fluxes for a materially advected region. A detailed circulation analysis of the non-advective fluxes for the WRF output is shown in Rutherford and Dunkerton (2017).

d. Lobes on isentropic surfaces

Due to the existence of the frontal boundary and large moisture and temperature gradient on the north side of the pouch, one may question whether manifolds computed with isobaric velocities represent realistic particle motions. The manifolds using isentropic velocities at the 315 K level, representative of the $\eta = 0.7$ level potential temperature during the genesis time period, are overlaid on the isentropic vorticity in Figure 5 (a)-(b). While some of the details of the manifolds change from the $\eta = 0.7$ level, the separatrix remains similar, with lobes L_1 from the dry region and L_3 from the southern moist region responsible for most of the transport from the environment into the pouch. The agreement of isentropic and isobaric manifold analyses is consistent with a hypothesis that the baroclinic characteristics of the frontal zone do not penetrate significantly into the immediate environment of Nate, that is, the inner pouch region. Such may not be the case for tropical storm formation in general, e.g., in tropical transition from a baroclinic precursor. However, the advantage of isentropic analysis is lost when parcel motions are no longer adiabatic on short time scales, as in regions of intermittent deep convection. We prefer isobaric analysis for this reason, irrespective of sloping isentropes, and for a more general reason that isobaric surfaces remain stratified (monotonic in height) everywhere in the atmosphere. Isentropic surfaces, on the other hand, are non-monotonic in breaking gravity waves and ill-defined in moist buoyant fields (convective clouds) and neutrally stratified dry boundary layer. Outcropping of isobaric surfaces in high topography or intense low pressure (e.g., hurricane) might be avoided with a sigma or hybrid coordinate, if desired, but it may be equally desirable to retain the isobaric formalism and to calculate pressure and frictional torques explicitly, together with trace constituent sources and sinks, along such physically constrained manifold boundaries. Issues associated with topography are thought to be second order effects in this study and consequently lie outside the scope of the present study.

e. Non-divergent lobe transport

Using the full flow field on constant η-surfaces, convergence leads to a net entrainment of vorticity contained in lobes, and it is not surprising that the area of the entrained lobes is far greater than the area of the expelled lobes. To further examine how the lobes are created, we again locate the manifolds using the non-divergent flow, computed using a Helmholtz decomposition on the WRF velocity fields. The manifolds are overlaid on the water vapor mixing ratio in Figure 5 (c)-(d). The hyperbolic trajectories are very similar to those in the divergent flow. The lobes on the north side of the pouch are still present, and result from velocity fluctuations along the frontal boundary, though their size is much smaller and these lobes do not become entrained into the core. The time-variation can also be seen by the folding of the unstable manifold near the western hyperbolic trajectory. However, the manifold configuration to the south of the pouch has changed as there are no longer lobes; in fact the time evolution of the unstable manifold shows a very slow time variation. While time-dependence of the rotational flow alone is sufficient for lobe transport along the frontal boundary, it is time-dependence of the divergent flow that is responsible for lobe transport to the south. This observation indicates that lobe transport is tied to convection and the fact that there are a pair of lobes entrained over approximately one day in the divergent flow leads us to question whether 2D lobe transport could be a response to the diurnal cycle of convection.

f. Effects of varying SSTs

The role of varying SSTs is investigated by an additional WRF simulation using temporally constant SSTs at the initial time of 0 UTC 6 Sept so that the upwelling that occurred from Nate has no feedback into the simulation. The manifolds at $\eta = 0.7$ are overlaid on the vorticity field in Figure 5 (e)-(f). With constant SSTs, the disturbance intensifies slightly more quickly, reaching a maximum $\eta = .7$ vorticity of 9.35×10^{-4} by 0 UTC 7 Sept. compared with a maximum of 8.75×10^{-4} for the varying SST case. Though the fine scale structure is slightly different, the higher SSTs do not cause a topological change in the manifold configuration at $\eta = 0.7$. At other levels, e.g. $\eta = 0.5$ and $\eta = 0.6$ (not shown), the manifolds to the north remain the same, but the manifolds to the south do not have additional intersections allowing moist air with high vorticity to be entrained. Both the varying SST simulation and constant SST simulation show similar system-scale convergence at $\eta = .7$, as the area of the pouch is reduced to .72 times it original size, see Figure 6 (a). The circulation (Figure 6(a)) and mean vorticity (Figure 6 (b)) are slightly higher for the constant SST simulation, indicating only a modest impact of the upwelling to storm intensity. Differences between the two simulations are similar at other levels as they are at $\eta = .7$.

The WRF simulations collectively demonstrate that varying SSTs, resolution, and divergence have little impact on manifold structure or on the contribution of the manifolds to the circulation since the small filaments emanating from the lobes contain very little circulation. The primary Lagrangian structures, L_1 to the north, L_2 to the south, and the pouch, remain robust features that are relatively insensitive to fine-scale variations. Analysis of the WRF simulations through the mid-troposphere (not shown) also supports these conclusions.

g. Vortex radial structure

We now consider the radial profiles of important kinematic quantities including the strain rates. Both OW and the sum of the squares of strain rates are translation invariant quantities, so they do not depend on the choice of translating Eulerian reference frame, while the strain rates depend individually on the choice of coordinate system. We orient the coordinate system along the direction given by the tangent to particle motion by the transformed velocities $(\tilde{u},\tilde{v})^T = T^{-1}\mathbf{u}$, where $T = \frac{1}{\|\mathbf{u}\|}[\mathbf{u},\mathbf{n}]$ and $\mathbf{n} = (-v,u)$ is the outward normal vector. The velocity gradient tensor in this coordinate system is given by

$$\nabla\tilde{\mathbf{u}} = T^{-1}\nabla\mathbf{u}T = \begin{pmatrix} \tilde{u}_{\|} & \tilde{u}_{\perp} \\ \tilde{v}_{\|} & \tilde{v}_{\perp} \end{pmatrix} \tag{7}$$

The shear and normal strain rates are given by $S_n = \tilde{u}_{\|} - \tilde{v}_{\perp}$ and $S_s = \tilde{v}_{\|} + \tilde{u}_{\perp}$ respectively, and satisfy $S_n^2 + S_s^2 = S_1^2 + S_2^2$. In this rotated coordinate, the strain rates are oriented parallel to the tangent vector (S_s) and normal to the tangent vector (S_n).

The time evolution of radial profiles for OW, shear strain, relative humidity, and vorticity from the ECMWF data is summarized in Figure 7 (a)-(d), respectively. The line marking the radius of the shear sheath, where the radial average of OW becomes negative, is shown as a function of time in white. The ζ time sequence shows higher average values toward the pouch center as time increases. Likewise, OW shows an increase near the center. As the vorticity is enhanced by vertical mass flux near the center, the strain regions outside the regions of high vorticity are advected inward toward the limit cycle, but remain just outside the region of highest vorticity. However, while ζ decreases slowly outside the center as the highest vorticity is concentrated in the core, the OW values show a dramatic decrease to negative values just outside the core due to higher strain. As the inward transport along the lobes progresses, the manifolds lengthen, increasing the area within the pouch that is dominated by strain. From Figure 7 (d), we see that as the unstable manifold is entrained near the center toward a small radius, elevated values of S_s appear just outside the strongest rotation at the radius where the unstable manifold is entrained. High OW and ζ values are present inside this radius as the flow is close to solid-body rotation. As it is entrained, the strain along the unstable manifold changes from stretching normal to the manifold to parallel shearing along the manifold. This shear boundary protects the vortex from further interaction with low-vorticity dry air, and allows concentration of high vorticity air near the center of the pouch. Thus, high OW values at the pouch center cannot occur without high strain just outside the region of high OW, and this radial profile of strain versus rotation are the leading indicator of higher ζ. The importance of the shear sheath can be seen in the relative humidity profile, Figure 7 (c), where radial averages of relative humidity are very high within the shear sheath, but the averages drop quickly outside the shear sheath.

h. Backward trajectories

Backward trajectories provide additional details about the impermeability of the inner core. Trajectories were seeded uniformly at 0 UTC 9 Sept. within the inner core boundary defined as a circle 1 degree of the storm center and advected backward in time isobarically to 1200 UTC 6 Sept. Their radius from the circulation center and θ_e values are plotted at 12 hour intervals in Figure 8 where the temporal positions are marked in different colors . The 500 hPa and 700 hPa backward trajectories are shown in panels (a) and (b), respectively, where orange dots inside a radius of 1 degree indicate that trajectories from the inner core on 0 UTC Sept. 9 were completely contained within the pouch boundary during the entire integration until 1200 UTC 6 Sept. None of these trajectories were significantly drier at earlier times, acquiring a θ_e increment of approximately 4-6 K at 500 hPa and 6-10 K at 700 hPa. During this gradual moistening trend, air is brought from over 3 degrees, but still within the pouch, to smaller radius in the core.

The 850 hPa and 925 hPa trajectories are shown in (c) and (d), and indicate that a portion of the trajectories originated from much drier regions, and moistened significantly during their entrainment. Many of these trajectories originated at locations further than 8 degrees from the center and their θ_e values increase by as much as 40 K coming inward toward center. Tracking the initial latitude of these trajectories (not shown) indicates that almost all of them came from north of the pouch, consistent with what is already known from the manifold locations. The moistening in the boundary layer associated with surface moisture fluxes over sea and entrainment from low-level convergence are not surprising. However, we see that a portion of the 850 hPa and 925 hPa trajectories are within 2 degrees of the center with θ_e values less than 330 K at 0 UTC 8 Sept., just prior to the period of weakening. At this time, Nate was over cooler water, and the entrained air was not moistened.

An idealized study by Braun et al. (2012) found that disturbances that reside very close to dry air and entrain dry air to within approximately 200 km of the circulation center may develop more slowly but achieve a similar maximum intensity. Our findings here indicate that the radial distance of entrainment from the center may not be the only factor limiting development, but whether the intrusion is able to penetrate the shear sheath. However, even without complete penetration, dry air may influence the storm by modifying the inflow layer as shown by Powell (1990) and Riemer and Montgomery (2011). An additional modeling study showing the different depths of entrainment of manifolds would be required to completely understand the implications of entrainment depth on development. Yablonsky and Ginis (2008) and Yablonsky and Ginis (2009) showed that oceanic upwelling may be a limiting factor in storm intensity also, and we suggest that it may have been a factor in Nate's weakening prior to landfall.

i. Horizontal transport at 500 hPa and 850 hPa

We now examine the vertical structure of the pouch by identifying the manifold structure on other levels. The manifolds are shown at 1800 UTC Sept. 6 to 0600 UTC Sept. 8 at 850 hPa (left column) and 500 hPa (right column) in Figure 9. These manifolds were identified by the same methods as those at 700 hPa, and the unstable manifolds show a configuration very similar to those at 700 hPa. The stable manifolds at the other levels have some important differences from those at 700 hPa.

At 500 hPa, the structure is very similar to the structure at 700 hPa, where the manifolds form a complete pouch boundary, and allow only a small intrusion of dry air from the north that is contained within a lobe. A very similar structure (not shown) can be observed at 400 hPa and 600 hPa, though it does not extend above 400 hPa.

At 850 hPa, the manifold structure differs from those found from 700 hPa to 500 hPa in that the stable manifolds do not have additional intersections with the unstable manifolds other than at the locations of hyperbolic trajectories. As the manifolds evolve, the northern unstable manifold is entrained inward, leaving a large region of dry air that can enter the vortex. Lobe

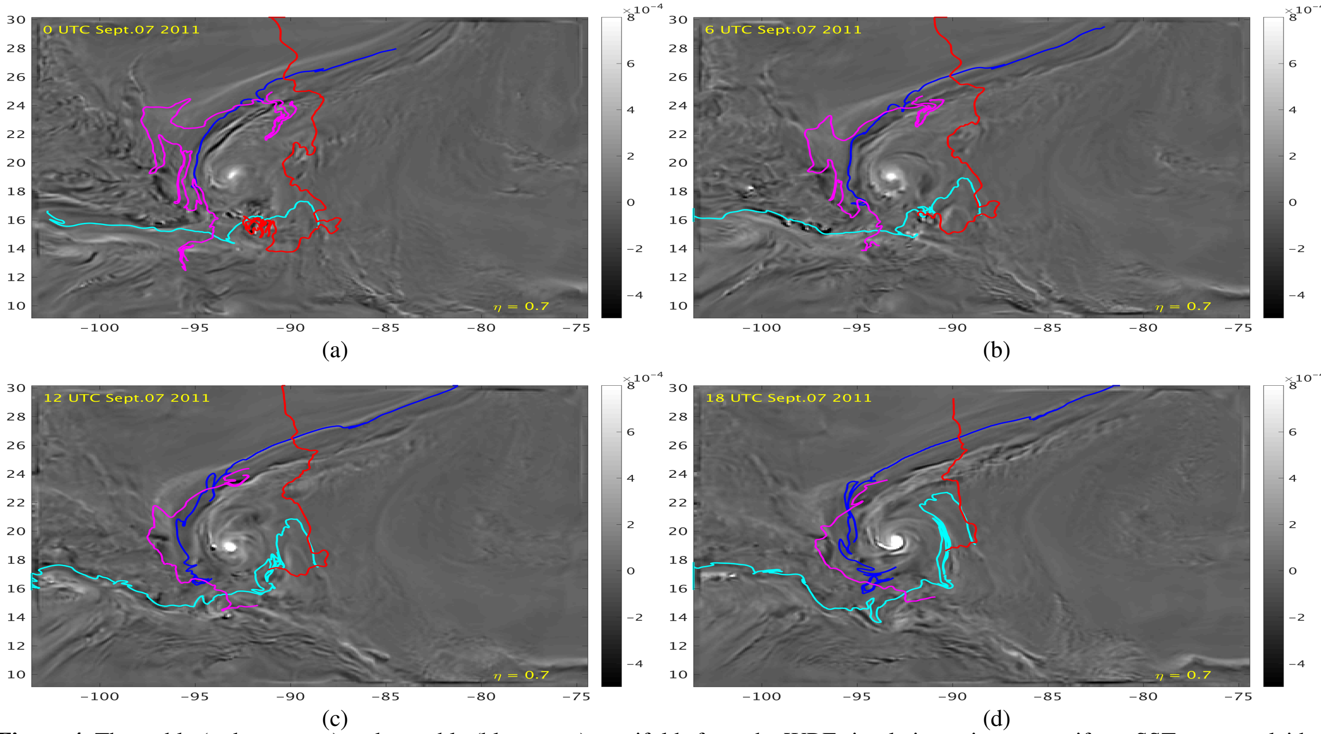

Figure 4. The stable (red, magenta) and unstable (blue, cyan) manifolds from the WRF simulation using non-uniform SSTs are overlaid on the vertical vorticity (s^{-1}) in (a-d).

transport does not apply here and entrainment of dry air is not limited to the contents of the lobes, but rather, the total flux through the open pathway.

At both 500 hPa and 850 hPa, unstable manifolds are entrained into a limit cycle of circular flow with no further entrainment, and like at 700 hPa, the change of hyperbolic to shear stability of the manifold forms a shear sheath that provides some protection to the inner core, defined kinematically as the region with strong recirculation seen, e.g., by large positive OW values, from the intruding dry air, Figure 9 (c)-(h). However, at 850 hPa, some dry air has been entrained into the inner core prior to the formation of the shear sheath at 1200 UTC 9 Sept., Figure 9 (c) and (e) (see also Figure 8 (c)). At 500 hPa, the shear sheath, seen by the limit cycle (cyan curve) at 0 UTC 9 Sept., is established prior to the entrainment of dry air.

5 Conclusions

In this paper, we have explored how the rearrangement of Lagrangian flow boundaries may limit the dry air in the vicinity of a tropical disturbance from interacting with the disturbance. Hurricane Nate developed despite a region of very dry air in close proximity to the storm. While the storm-relative frame showed closed streamlines, the stable and unstable manifolds defined invariant regions called lobes that can transport intruding dry air into the pouch toward the storm center, but failed to penetrate

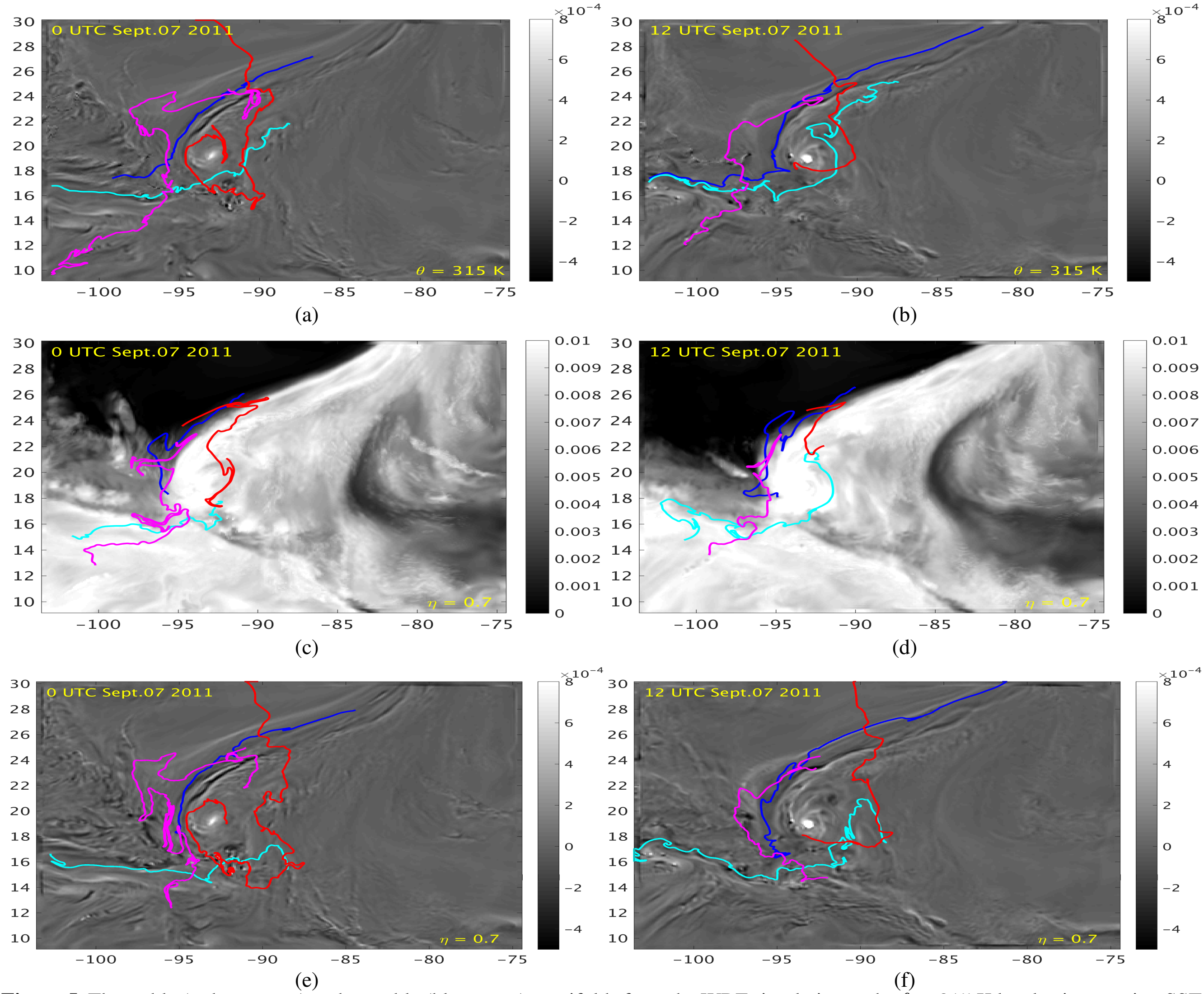

Figure 5. The stable (red, magenta) and unstable (blue, cyan) manifolds from the WRF simulation at the $\theta = 315$ K level using varying SSTs are overlaid on the vertical vorticity (s^{-1}) in (a-b), manifolds from the non-divergent velocity field from the WRF varying SST simulation are overlaid on the water vapor mixing ratio (g/kg) in (c-d), and manifolds at the $\eta = 0.7$ level using constant SSTs are overlaid on the vertical vorticity (s^{-1}) in (e-f).

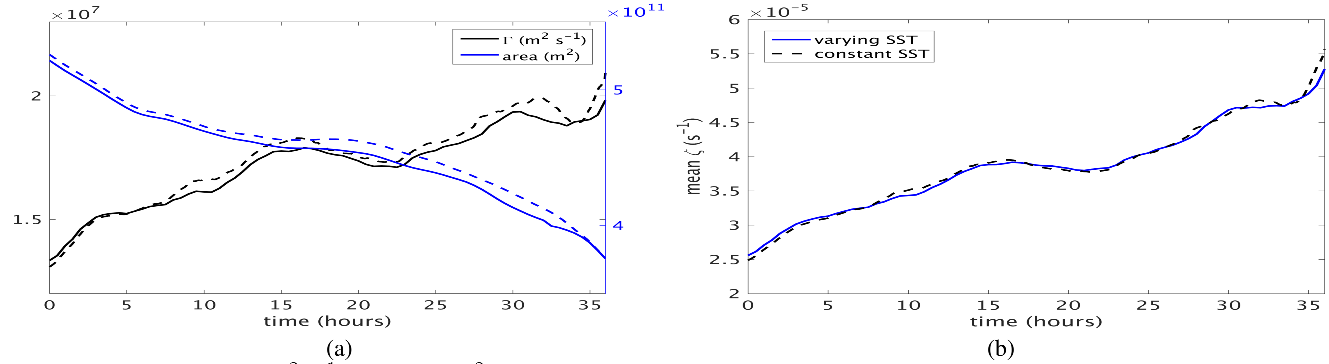

Figure 6. The circulation (m^2s^{-1}) and area (m^2) are shown in (a) as black and blue curves resp. for the varying SST (solid lines) and constant SST (dashed lines) WRF simulations, respectively. The mean vorticity (s^{-1}) is shown in (b) for the varying SST simulation (solid) and constant SST simulation (dashed).

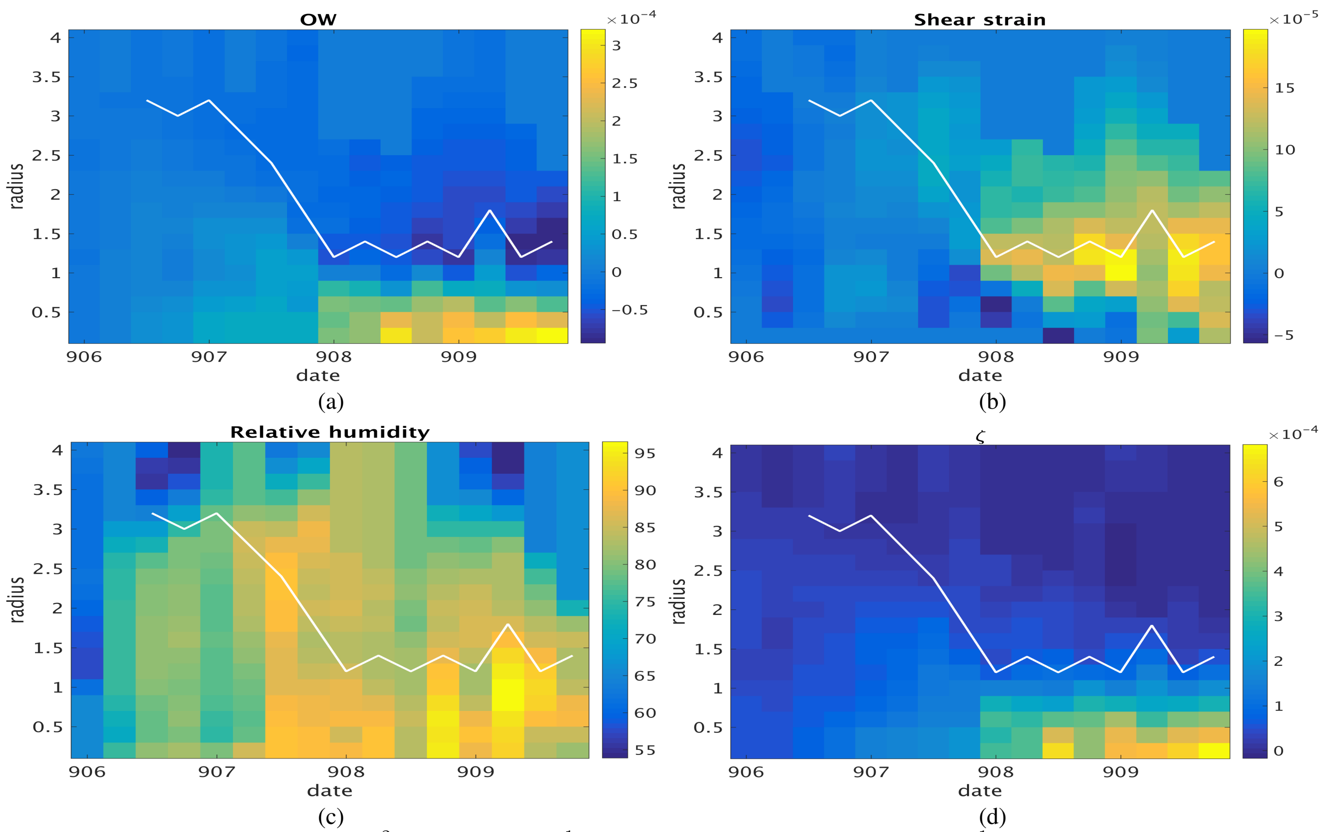

Figure 7. The radial profiles of OW (s^{-2}), shear strain (s^{-1}), relative humidity (%), and vorticity (s^{-1}) from the ECMWF data are shown in (a)-(d), respectively, from Sept. 0600 to 1800 UTC Sept. 9. The radial location of the shear sheath is shown in white.

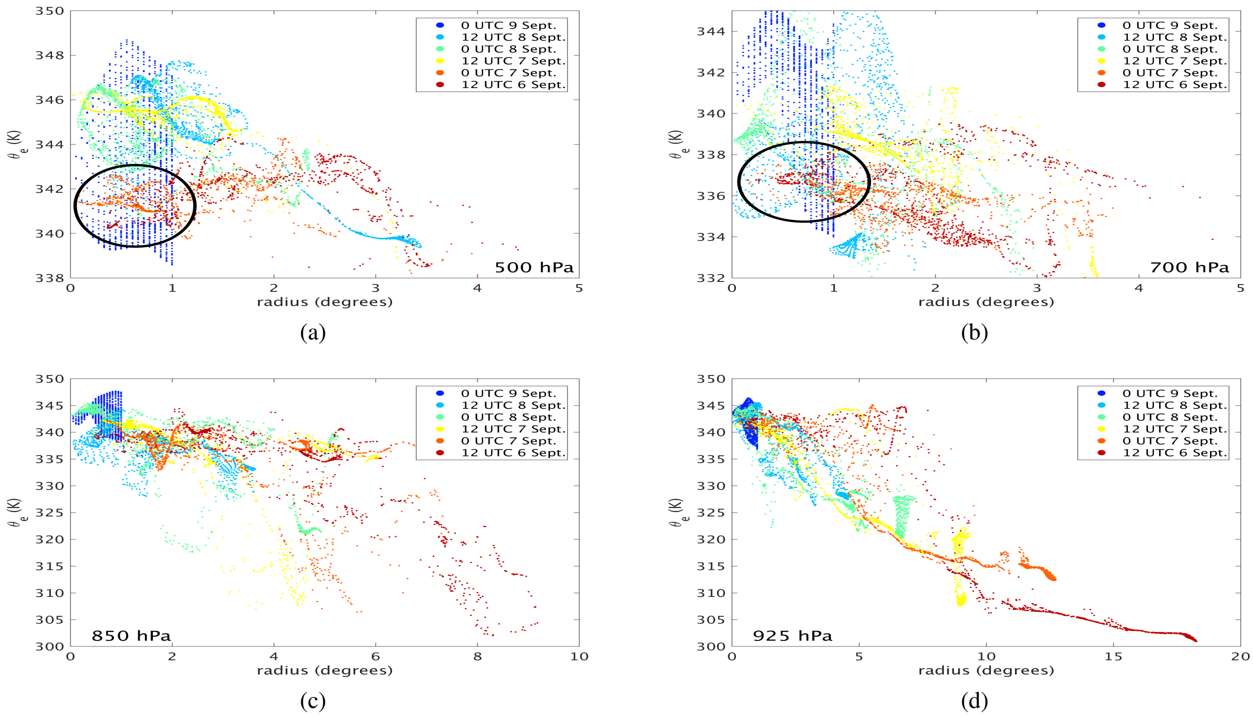

Figure 8. The values of θ_e versus radius from circulation center are plotted for sets of isobaric trajectories from the ECMWF data released within the inner core boundary at 0 UTC 9 Sept. and integrated backward to 1200 UTC 6 Sept. at 500 hPa, 700 hPa, 850 hPa, and 925 hPa in (a)-(d) resp. The different colors indicate the time at which the properties of the trajectories were analyzed. Sets of trajectories that remain in the core during the entire integration are located inside the black ellipse in (a) and (b).

the core of the proto-vortex. A shear sheath served to protect the center by maintaining a strongly deforming radial shear which, in turn, allowed vorticity concentration of the core to continue, undiluted with dry air and weaker vorticity.

We offered a dynamic view of the pouch for Nate that describes the entire storm evolution at fixed vertical (e.g. isobaric) levels based on the evolution of Lagrangian flow boundaries. In this view, we found that the Lagrangian pouch structure showed the sources of air that were advected into the pouch. We also showed that the advective fluxes of vorticity into the pouch can be measured by lobe transport, and account for over half of the vorticity that Nate acquired. The transport that we see in this case is consistent with the radial profiles which showed the accumulation of the manifolds, an increasing tracer gradient, and a shear sheath that marks an additional transport boundary to the inner core.

When Nate was a tropical storm in close proximity to dry air, the entrainment of dry air was limited to what was transported by lobes when an enclosed Lagrangian boundary was present.

The Lagrangian boundaries lead us to a material description of the transition from a large-scale pouch boundary that blocks environmental dry air during genesis to a much smaller vortex core that is present after genesis:

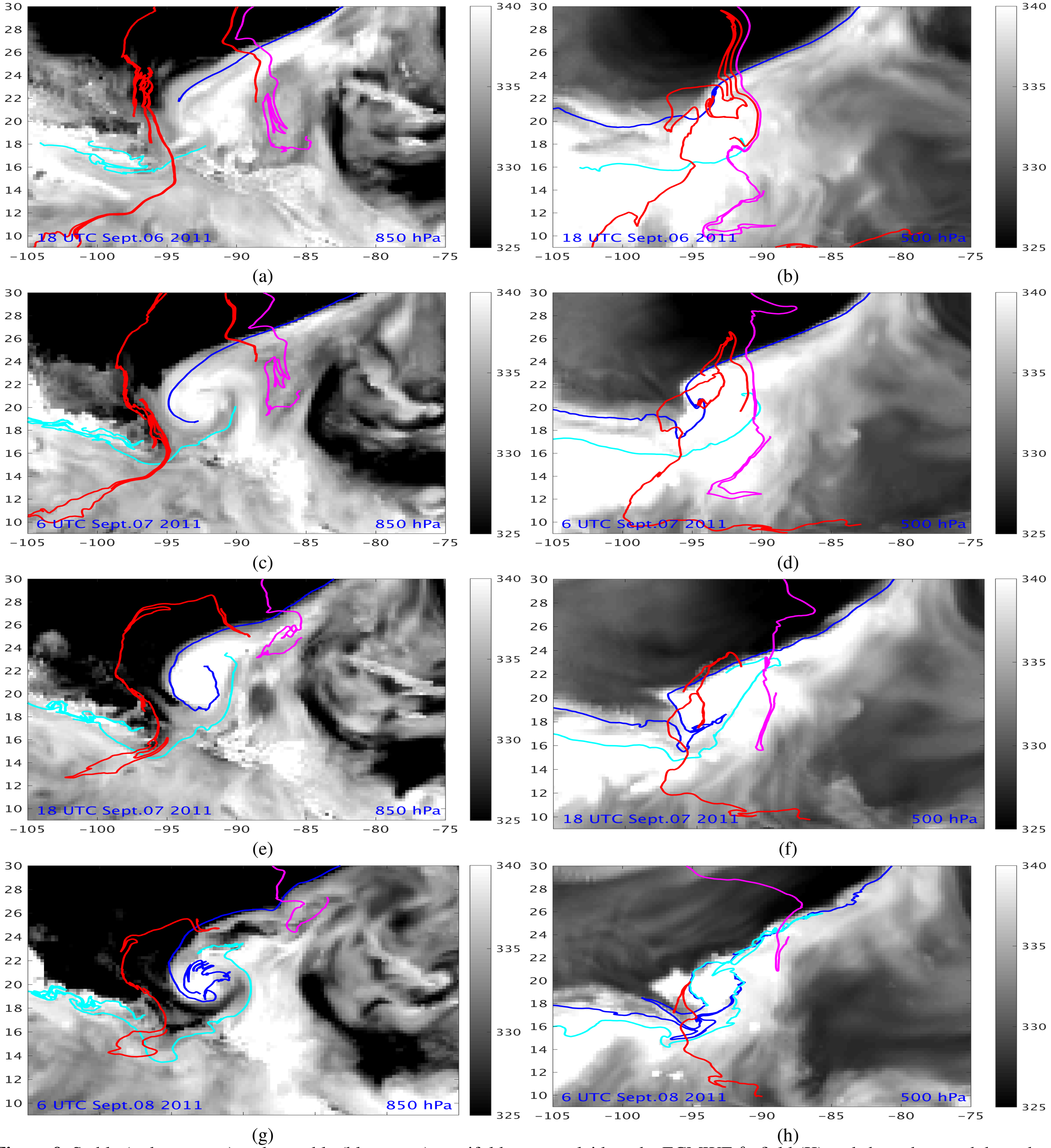

Figure 9. Stable (red, magenta) and unstable (blue, cyan) manifolds are overlaid on the ECMWF θ_e field (K) and show the pouch boundary from 1800 UTC Sept. 6 to 0600 UTC Sept. 8 at 850 hPa (left) and 500 (right) hPa.

1. The frontal boundary rolls up and combines two air masses, one from each side of the frontal boundary.

2. During the rollup, hyperbolic trajectories become detectable along the boundary, indicating the existence of stable and unstable manifolds.

3. Additional intersection points of the manifolds that are not the hyperbolic trajectories travel cyclonically toward the hyperbolic trajectory, and the manifold segments between adjacent intersection points mark the lobe boundaries.

4. Within the pouch, wrapping of the unstable manifold reaches a limit cycle surrounding the inner core as convergence concentrates vorticity from the moist region into a vortex core.

5. In a competing process, additional entrainment of lobes allows the import of dry air towards, but not necessarily into, the core.

6. As vorticity is concentrated into the core, the unstable manifold lengthens, and the elongated manifolds and lobes form a shear sheath barrier to transport of additional dry air into the core[8].

There are two configurations of manifolds that describe the transport of dry air toward the storm center along the manifolds. At 700 hPa and 500 hPa, lobe transport and a rearrangement of a separatrix allowed a region of dry air to enter the pouch though streamlines remained closed. However, the dry air region was contained and did not penetrate the inner core boundary due to the presence of the shear sheath. At 850 hPa, the manifolds showed that there was a direct pathway of transport into the pouch that still reached a limit cycle before reaching the circulation center, and the pathway was wider than suggested by translating Eulerian streamlines. These two mechanisms for dry air transport compete with the aggregation of cyclonic vorticity. Lobe transport is a slower process which limits the amount of dry air entering the vortex, while an open pathway allows continual entrainment of dry air.

Based on companion numerical integrations of this case, the advection of manifolds is somewhat sensitive to SST, pressure level, integration time and numerical model (details). While the fine-scale details of the manifolds may differ considerably, the differences between manifolds computed in different ways are confined to filaments that have little circulation and are homogenized. The conclusion, that dry air from the north of Nate entered in and corresponded to the transport of one lobe, while moist air that entered Nate was confined to another lobe, is robust.

Further study on the rate of entrainment versus the rate of vorticity aggregation in an idealized setting and in modeling studies will help clarify the role of dry air intrusions that are partially ingested into developing storms in slowing but still allowing development. The techniques used here should be useful for those studies.

[8]In this case, entrainment of manifolds forms a transport barrier at the edge of the inner core where the entrainment of lobes is due to time-dependence of velocities. The end result is similar to the effect of divergence in steady flow studied in Riemer and Montgomery (2011). Alternatively, Rutherford et al. (2012) found that the remnant manifolds exterior to VHT's may help to form the boundary without being attached to a hyperbolic trajectory at the edge of the pouch. These processes are not mutually exclusive and the shear sheath is a combination of these processes.

Acknowledgments

The authors would like to acknowledge NSF grants AGS-1313948, AGS-1439283, AGS-0733380 (now expired), and NASA grant NNG11PK021. The authors would also like to thank Drs. Gerard Kilroy and Roger Smith and the German Weather Service for providing us with the ECMWF global model data for this basic research investigation.

References

Avila, L. and S. Stewart, 2013: Atlantic Hurricane Season of 2011. *Mon. Wea. Rev.*, **141**, 2577–2596.

Babiano, A., G. Boffetta, A. Provenzale, and A. Vulpiani, 1994: Chaotic advection in point vortex models and two-dimensional turbulence. *Phys. Fluids*, **6 (7)**, 2465–2474.

Beron-Vera, F. J., M. J. Olascoaga, M. G. Brown, H. Koçak, and I. I. Rypina, 2010: Invariant-tori-like Lagrangian coherent structures in geophysical flows. *Chaos*, **20 (1)**, 017 514, doi:10.1063/1.3271342, http://www.ncbi.nlm.nih.gov/pubmed/20370304.

Branicki, M., A. Mancho, and S. Wiggins, 2011: A Lagrangian description of transport associated with a front-eddy interaction: Application to data from the north-Western Mediterranean Sea. *Physica D*, **240 (3)**, 282–304, http://www.sciencedirect.com/science/article/pii/S0167278910002538.

Braun, S., J. Sippel, and D. Nolan, 2012: The Impact of Dry Midlevel Air on Hurricane Intensity in Idealized Simulations with No Mean Flow. *Journal of the Atmospheric Sciences*, **69 (1)**, 236–257, doi:10.1175/JAS-D-10-05007.1, http://journals.ametsoc.org/doi/abs/10.1175/JAS-D-10-05007.1.

Davis, C. and D. Ahijevych, 2012: Mesoscale Structural Evolution of Three Tropical Weather Systems Observed during PREDICT. *Journal of the Atmospheric Sciences*, **69 (4)**, 1284–1305, doi:10.1175/JAS-D-11-0225.1, http://journals.ametsoc.org/doi/abs/10.1175/JAS-D-11-0225.1.

Duan, J. and S. Wiggins, 1996: Fluid Exchange across a Meandering Jet Quasiperiodic Variability. *Journal of Physical Oceanography*, **26 (7)**, 1176–1188, http://authors.library.caltech.edu/12258/.

Dunkerton, T. J., M. T. Montgomery, and Z. Wang, 2009: Tropical cyclogenesis in a tropical wave critical layer : easterly waves. *Atmospheric Chemistry and Physics*, **9 (15)**, 5587–5646, doi:10.5194/acp-9-5587-2009, http://adsabs.harvard.edu/abs/2009ACP.....9.5587D.

Farazmand, M. and G. Haller, 2012: Computing Lagrangian coherent structures from their variational theory. *Chaos (Woodbury, N.Y.)*, **22 (1)**, 013 128, doi:10.1063/1.3690153, http://www.ncbi.nlm.nih.gov/pubmed/22463004.

Frank, N., 1970: Atlantic tropical systems. *Mon. Wea. Rev.*, **98**, 307–314.

Freismuth, T., B. Rutherford, M. A. Boothe, and M. T. Montgomery, 2016: Why did the storm ex-Gaston (2010) fail to redevelop during the PREDICT experiment?. *Atmos. Chem. Phys.*, **(16)**, 1–9, doi:10.5194/acp-16-1-2016.

Gray, W., 1968: Global view of the origin of tropical disturbances and storms. *Mon. Wea. Rev.*, **96**, 669–700.

Haller, G. and Hadjighasem, A. and Farazmand, M. and Huhn, F., 2015: Defining Coherent Vortices Objectively from the Vorticity.

Haynes, P. and M. McIntyre, 1987: On the evolution of vorticity and potential vorticity in the presence of diabatic heating and frictional or other forces. *Journal of the Atmospheric Sciences*, **44 (5)**, 828–841, doi:10.1175/1520-0469(1987)044<0828:OTEOVA>2.0.CO;2, http://journals.ametsoc.org/doi/abs/10.1175/1520-0469(1987)044<0828:OTEOVA>2.0.CO;2.

Haynes, P. H. and M. E. McIntyre, 1990: On the conservation and impermeability theorems for potential vorticity. *Journal of the Atmospheric Sciences*, **47 (16)**, 2021–2031, doi:10.1175/1520-0469(1990)047<2021:OTCAIT>2.0.CO;2, http://www.atm.damtp.cam.ac.uk/mcintyre/haynes-mci90.pdfhttp://journals.ametsoc.org/doi/abs/10.1175/1520-0469(1990)047<2021:OTCAIT>2.0.CO;2.

Ide, K., D. Small, and S. Wiggins, 2002: Distinguished hyperbolic trajectories in time-dependent fluid flows: analytical and computational approach for velocity fields defined as data sets. *Nonlinear Processes in Geophysics*, **9**, 237–263, http://hal.archives-ouvertes.fr/hal-00302110/.

Joseph, B. and B. Legras, 2002: Relation between Kinematic Boundaries, Stirring, and Barriers for the Antarctic Polar Vortex. *Journal of the Atmospheric Sciences*, **59 (7)**, 1198–1212, doi:10.1175/1520-0469(2002)059<1198:RBKBSA>2.0.CO;2, http://journals.ametsoc.org/doi/abs/10.1175/1520-0469(2002)059<1198:RBKBSA>2.0.CO;2.

Killworth, P. D. and M. E. McIntyre, 1985: Do Rossby-wave critical layers absorb, reflect, or over-reflect? *Journal of Fluid Mechanics*, **161 (-1)**, 449, doi:10.1017/S0022112085003019, http://journals.cambridge.org/production/action/cjoGetFulltext?fulltextid=391434.

Kilroy, G. and R. K. Smith, 2013: A numerical study of rotating convection during tropical cyclogenesis. *Quarterly Journal of the Royal Meteorological Society*, **139 (674)**, 1255–1269, doi:10.1002/qj.2022, http://doi.wiley.com/10.1002/qj.2022.

Koh, T. and B. Legras, 2002: Hyperbolic lines and the stratospheric polar vortex. *Chaos Woodbury Ny*, **12 (2)**, 382–394, doi:10.1063/1.1480442, http://www.ncbi.nlm.nih.gov/pubmed/12779568.

Koh, T. and R. Plumb, 2000: Lobe dynamics applied to barotropic Rossby-wave breaking. *Physics of Fluids*, **12 (6)**, 1518, doi:10.1063/1.870400, http://link.aip.org/link/PHFLE6/v12/i6/p1518/s1&Agg=doi.

Lapeyre, G., P. Klein, and B. Hua, 1999: Does the tracer gradient vector align with the strain eigenvectors in 2D turbulence? *Physics of Fluids*, **11 (12)**, 3729–3737, http://link.aip.org/link/PHFLE6/v11/i12/p3729/s1.

Lapeyre, G., 2002: Characterization of finite time Lyapunov exponents and vectors in two-dimensional turbulence *Chaos*, **12 (3)**, 688–698.

Lussier, L., B. Rutherford, M. Montgomery, T. Dunkerton, and M. Boothe, 2015: Examining the Roles of the Easterly Wave Critical Layer and Vorticity Accretion during the Tropical Cyclogenesis of Hurricane Sandy. *Monthly Weather Review*, **143 (5)**, 1703–1722, doi:10.1175/MWR-D-14-00001.1.

Malhotra, N. and S. Wiggins, 1998: Geometric Structures, Lobe Dynamics, and Lagrangian Transport in Flows with Aperiodic Time-Dependence, with Applications to Rossby Wave Flow. *Journal of Nonlinear Science*, **8 (4)**, 401–456, doi:10.1007/s003329900057, http://www.springerlink.com/openurl.asp?genre=article&id=doi:10.1007/s003329900057.

Mancho, A., E. Hernandez-Garcia, D. Small, S. Wiggins, and V. Fernandez, 2006a: Lagrangian transport through an ocean front in the North-Western Mediterranean Sea. *Journal of Physical Oceanography*, **38 (6)**, 34, http://arxiv.org/abs/physics/0608105.

Mancho, A., D. Small, and S. Wiggins, 2006b: A tutorial on dynamical systems concepts applied to Lagrangian transport in oceanic flows defined as finite time data sets: Theoretical and computational issues. *Physics Reports*, **437 (3-4)**, 55–124, doi:10.1016/j.physrep.2006.09.005, http://linkinghub.elsevier.com/retrieve/pii/S0370157306003401.

Mancho, A., D. Small, S. Wiggins, and K. Ide, 2003: Computation of stable and unstable manifolds of hyperbolic trajectories in two-dimensional, aperiodically time-dependent vector fields. *Physica D: Nonlinear Phenomena*, **182 (3-4)**, 188–222, doi:10.1016/S0167-2789(03)00152-0, http://linkinghub.elsevier.com/retrieve/pii/S0167278903001520.

McBride, J. and R. Zehr, 1981: Observational analysis of tropical cyclone formation Part II: Comparison of non-developing versus developing systems. *Journal of Atmospheric Sciences*, **38**, 1132–1151.

McWilliams, J., 1984: The emergence of isolated coherent vortices in turbulent flow. *Journal of Fluid Mechanics*, **146**, 21–43.

Miller, P., C. Jones, A. Rogerson, and L. Pratt, 1997: Quantifying transport in numerically generated velocity fields. *Physica D: Nonlinear Phenomena*, **110 (1-2)**, 105–122, http://www.sciencedirect.com/science/article/pii/S0167278997001152.

Montgomery, M., et al., 2012: The Pre-Depression Investigation of Cloud-Systems in the Tropics (PREDICT) Experiment: Scientific Basis, New Analysis Tools, and Some First Results. *Bulletin of the American Meteorological Society*, **93 (2)**, 153–172, doi:10.1175/BAMS-D-11-00046.1, http://journals.ametsoc.org/doi/abs/10.1175/BAMS-D-11-00046.1.

Ottino, J. M., 1990: The Kinematics of Mixing: Stretching, Chaos, and Transport., Cambridge - New York - New Rochelle 1989. XIV, 364 pp. *Cambridge University Press*, doi:10.1002/cite.330620126, http://doi.wiley.com/10.1002/cite.330620126.

Powell, M., 1990: Boundary layer structure and dynamics in outer hurricane rainbands. Part ii: Downdraft modification and mixed layer recovery. . *Mon. Wea. Rev.*, **118**, 918–938.

Riemer, M. and M. Montgomery, 2011: Simple kinematic models for the environmental interaction of tropical cyclones in vertical wind shear. *Atmospheric Chemistry and Physics*, **11**, 9395–9414.

Rodrigue, S. and E. Eschenazi, 2010: Lobe transport analysis of the Kelvin-Stuart cat's eyes driven flow. *Chaos (Woodbury, N.Y.)*, **20 (1)**, 013 101, doi:10.1063/1.3272714, http://www.ncbi.nlm.nih.gov/pubmed/20370256.

Rogerson, A., P. Miller, L. Pratt, and C. Jones, 1999: Lagrangian Motion and Fluid Exchange in a Barotropic Meandering Jet. *Journal of Physical Oceanography*, **29**, 2635–2655, http://journals.ametsoc.org/doi/abs/10.1175/1520-0485(1999)029<2635:LMAFEI>2.0.CO;2.

Rom-Kedar, V., A. Leonard, and S. Wiggins, 1990: An analytical study of transport, mixing and chaos in an unsteady vortical flow. *Journal of Fluid Mechanics*, **214**, 347–394, http://journals.cambridge.org/production/action/cjoGetFulltext?fulltextid=380626.

Rutherford, B., G. Dangelmayr, and M. T. Montgomery, 2012: Lagrangian coherent structures in tropical cyclone intensification. *Atmospheric Chemistry and Physics*, **12 (12)**, 5483–5507, doi:10.5194/acp-12-5483-2012, http://www.atmos-chem-phys.net/12/5483/2012/.

Rutherford, B. and T. Dunkerton, 2017: Finite-time corculation changes from topoligical rearrangement of distinguished curves and non-advective fluxes . *J. Atmos. Sci.*, submitted.

Rutherford, B., T. J. Dunkerton, and M. T. Montgomery, 2015: Lagrangian vortices in developing tropical cyclones. *Q. J. R. Meteorol. Soc.*, **141 (693)**, 3344–3354, doi:10.1002/qj.2616.

Rutherford, B. and M. Montgomery, 2012: A Lagrangian analysis of a developing and non-developing disturbance observed during the PREDICT experiment. *Atmospheric Chemistry and Physics*, **12**, 11 355–11 381, doi:doi:10.5194/acp-12-1-2012.

Samelson, R. and S. Wiggins, 2006: *Lagrangian transport in geophysical jets and waves: The dynamical systems approach*. Springer Verlag.

Serra, M. and G. Haller, 2016: Objective Eulerian Coherent Structures. *Chaos*, **26**, 053110, doi:10.1063/1.4951720.

Wiggins, S., 1992: *Chaotic Transport in Dynamical Systems*, Interdisciplinary applied mathematics, Vol. 45. Springer-Verlag, 68 pp., doi:10.1063/1.2809741, http://link.aip.org/link/PHTOAD/v45/i7/p68/s1&Agg=doi.

Wiggins, S., 2005: The Dynamical Systems Approach To Lagrangian Transport in Oceanic Flows. *Annual Review of Fluid Mechanics*, **37 (1)**, 295–328, doi:10.1146/annurev.fluid.37.061903.175815, http://www.annualreviews.org/doi/abs/10.1146/annurev.fluid.37.061903.175815.

Wiggins, S. and J. M. Ottino, 2004: Foundations of chaotic mixing. *Philosophical Transactions of the Royal Society - Series A: Mathematical, Physical and Engineering Sciences*, **362 (1818)**, 937–970, http://www.ncbi.nlm.nih.gov/pubmed/15306478.

Yablonsky, R. M. and I. Ginis, 2008: Improving the Ocean Initialization of Coupled Hurricane?Ocean Models Using Feature-Based Data Assimilation. *Monthly Weather Review*, **136 (7)**, 2592–2607, doi:10.1175/2007MWR2166.1, http://journals.ametsoc.org/doi/abs/10.1175/2007MWR2166.1.

Yablonsky, R. M. and I. Ginis, 2009: Limitation of One-Dimensional Ocean Models for Coupled Hurricane?Ocean Model Forecasts. *Monthly Weather Review*, **137 (12)**, 4410–4419, doi:10.1175/2009MWR2863.1, http://journals.ametsoc.org/doi/abs/10.1175/2009MWR2863.1.